Power System Coherency Identification Using Nonlinear Koopman Mode Analysis

Ahmad Anan Tbaileh

Thesis submitted to the faculty of Virginia Polytechnic Institute and State University in partial fulfillment of the requirements of the degree of

Master of Science

In
Electrical and Computer Engineering

Lamine M. Mili, Chair
C. Yaman Evrenosoğlu
William T. Baumann

May 2nd 2014
Falls Church, VA

Keywords: power system stability, coherency identification, modal analysis, model reduction, Koopman modes analysis (KMA)

Power System Coherency Identification Using Nonlinear Koopman Mode Analysis

Ahmad Anan Tbaileh

ABSTRACT

In this thesis, we apply nonlinear Koopman mode analysis to decompose the swing dynamics of a power system into modes of oscillation, which are identified by analyzing the Koopman operator, a linear infinite-dimensional operator that may be defined for any nonlinear dynamical system. Specifically, power system modes of oscillation are identified through spectral analysis of the Koopman operator associated with a particular observable. This means that they can be determined directly from measurements. These modes, referred to as Koopman modes, are single-frequency oscillations, which may be extracted from nonlinear swing dynamics under small and large disturbances. They have an associated temporal frequency and growth rate. Consequently, they may be viewed as a nonlinear generalization of eigen-modes of a linearized system. Koopman mode analysis has been also applied to identify coherent swings and coherent groups of machines of a power system. This will allow us to carry out a model reduction of a large-scale system and to derive a precursor to monitor the loss of transient stability.

Acknowledgement

I would like to extend my gratitude to Dr. Mili, without whose guidance and support this work would not have been possible. Dr. Evrenosoğlu created a perfect learning environment to strengthen my concepts which helped broaden my scope of thinking. I would like also to thank Dr. Baumann for his immense support and valuable feedback about this project.

My very special thanks to my parents whom I owe everything I am today. Their faith and confidence in my abilities and in me is what has shaped me to be the person I am today. Thank you for everything.

Table of Contents

List of Figures

List of Tables

Acronyms

KMA - Koopman Mode Analysis

KM - Koopman Mode

AVR - Automatic Voltage Regulator

ANN - Artificial Neural Network

SMA - Selective Modal Analysis

HSA - Hilbert Spectral Analysis

POD - Proper Orthonormal Decomposition

DFT - Discrete Fourier Transform

CSI - Coherent Swing Instability

Chapter 1 – Introduction

1.1 Problem statement

Power system stability is a research problem of increasing consideration among power researchers. This is due to the fact power systems are becoming more vulnerable to disturbances due to the continuous growth of load demand and the concomitant increase in generation capacity, which in turn results in an increase of transmission system loading. Power systems are characterized by complex phenomena that occur on large scales in both space and time. Examples of such phenomena are loss of synchronism of rotating machines, voltage dynamics and collapse, and cascading failures leading to widespread blackouts. Simulations of nonlinear mathematical models of power systems have revealed the possible occurrence of complex dynamics such as sustained oscillation [1], inter-area oscillations [2], chaotic oscillations [3], which may lead to cascading failures and blackouts [4].

Power systems experience different types of modes of oscillation that are excited by a disturbance, depending on its strength and location and the topology of the system. Examples of such modes are inter-area modes of oscillation, local modes of oscillation [5] and Koopman modes, which will be discussed in this thesis.

If not properly damped, these oscillatory modes can grow larger to the point to destabilize the system. This can result from generators stepping out of synchronism, sequence of line outages, and voltage collapse. Analyzing these modes of oscillation can help us to understand the behavior of the system under stress and to propose mitigation measures. They can be utilized to design controllers to damp the oscillations, or provide the control center operators with precursor of transient instability to take preventive actions.

Because power systems are large-scale systems (e.g., eastern US connection has more than 60,000 buses) and have different types of nonlinearities, their dynamics are difficult to model and analyze. The linear analysis that is usually carried out to investigate power system linear

modes of oscillation hinges on model linearization at equilibria and the application of linear system theories and methods. In the case where the system operating point remains in the vicinity of a stable equilibrium point, which is obtained from the steady-state power flow analysis, this linear approximation is valid and the analysis will give reliable results. However, when the power system is experiencing a large disturbance, which will pull the system operating point far away from a stable equilibrium point, termed attractor, a linear approximation may not be valid since nonlinear interactions that the system may experience are disregarded from the analysis.

1.2 Objective of the study

The aim of this study is to apply Koopman mode analysis in power systems. This is a method that decomposes a system into modes of oscillation based on system observables. These modes have associated single frequencies and growth rates, which can be seen as a nonlinear generalization of the eigenmodes of a linearized system. The Koopman operator is a linear operator defined for any nonlinear systems. Though the dynamics of the system are finite-dimensional, a Koopman operator lies on an infinite-dimensional space, does not rely on linearization, and captures the full information about the nonlinear dynamics of a system.

In this thesis, this method has been described and applied in power systems to decompose the system into a set of dominant modes of oscillation. A comparison has been carried out between Koopman mode analysis and the more traditional small-signal stability analysis. For both methods, we have compared modes of oscillation and the identification of coherent groups of machines. We have also investigates the effect of fault location on the coherent grouping of machines. Another examination has been carried out to check the impact that generators models may have on modal analysis. In addition to the coherency analysis, a reduced-order model has been developed to investigate power system stability.

1.3 Contributions

We have provided a detailed discussion of Koopman mode analysis. This method has been applied to two different systems, namely the four-machine two-area system, and the IEEE 39-bus system. A comparison has been made between the KMA and the conventional small-signal stability analysis on the 4-machine test system in terms of modal analysis and identification of frequencies of oscillation. It has been found that KMA and small-signal stability analysis give very similar results when the system experiences small disturbances. However, this is no longer true for large disturbances. Since small-signal stability relies on linearization, it neglects all nonlinearities in the system, which is not the case for KMA. Simulations carried out on the 39-bus system revealed that the Koopman modes depend on the location of the disturbance. Two different models for the generators were used to investigate the impact that generator models have on KMA, especially AVR. Specifically, we have investigated the simple classical model and the two-axis model with a fast exciter, namely the IEEE-Type-I excitation system. It has been shown that the use of more complex models such as the two-axis or the flux-decay model will only affect the damping of system dynamics while slightly modifying the frequencies of the oscillations. It has been concluded that the classical generator model is sufficient to capture the modes of oscillation and identify the coherent machines. A model reduction technique using the dominant modes has been derived and utilized to investigate the performance of power system dynamics. The action-angle representation has been developed to derive a precursor to system instability. This representation hinges on a set of KMs obtained from the first few seconds following a disturbance and before the system experiences instability. It has been observed that system instability occurs when the amplitude of one of the modes starts to grow until it destabilizes the other modes. An index of instability can be derived by comparing these amplitudes to a threshold.

1.4 Outline of the Thesis

The outline of the thesis will be as follows. In chapter 2 the different models for the generators used in the study will be described and a brief literature review for power system stability, coherency identification and modal analysis approaches will be provided. In chapter 3 the Koopman mode theory will be discussed in details with its applications to power systems. In chapter 4 two case studies will be used to demonstrate the Koopman analysis technique and its applications in terms of modal analysis, coherency identification and model reduction to assess the power system stability. In chapter 5, the findings of the thesis will be summarized and future work will be discussed.

Chapter 2 – Power System Stability Modeling and Analysis

In this chapter, we provide the classical and the two-axis models of a synchronous machine and briefly review power system stability and the conventional coherency and modal analysis techniques, including small-signal stability analysis, the proper orthonormal decomposition technique, and the Hilbert-spectral analysis methods.

2.1 Power system Models

The general form of the power system dynamic equations can be expressed by

$$\begin{aligned} \underline{\dot{x}} &= \underline{f}\left(\underline{x}, \underline{y}, \underline{u}\right), \\ \underline{0} &= \underline{g}\left(\underline{x}, \underline{y}\right), \end{aligned} \tag{1}$$

where:

f: the differential equations representing the generators internal dynamics and controllers,

g: the stator and network algebraic equations,

x: the vector of the system states,

y: a vector which includes the machines stator currents I and the complex terminal voltages V,

u: the input vector to the system,

Here we will use two models for representing the generators, the classical model and the two-axis model. Considering a system with n buses and m machines, for the classical model the differential equations of the generators can be expressed as

$$\begin{aligned} &\frac{d\delta_i}{dt} = \omega_i - \omega_s\,, \\ &M_i \frac{d\omega_i}{dt} = T_{Mi} - \sum_{j=1}^{n} E_i E_j (G_{ij} cos\delta_{ij} + B_{ij} sin\delta_{ij}) - D_i(\omega_i - \omega_s), \end{aligned} \tag{2}$$

where: $i = 1, \dots, m$,

δ_i: Generator's rotor angle,

ω_i: Generator's speed,

T_{Mi}: Input mechanical torque applied to the shaft,

M_i: Inertia constant,

E_i: Generator's internal bus voltage,

G_{ij}: Transmission line conductance,

B_{ij}: Transmission line susceptance,

D_i: Damping ratio.

Here, we will model the loads as constant impedances. This will allow reducing the network to the generators internal buses, and the system will be represented only by the differential equations, without the network algebraic equations. Therefore, the final model of the system (1) will be

$$\underline{\dot{x}} = \underline{f}(\underline{x}), \tag{3}$$

where $x = (\delta_1, \dots \delta_m, \omega_1, \dots, \omega_m)$,

For the two-axis model [6], the differential equations expressing the dynamics of the machines, including a first order exciter model, are:

$$\frac{d\delta_i}{dt} = \omega_i - \omega_s \ , \tag{4}$$

$$\frac{d\omega_i}{dt} = \frac{T_{Mi}}{M_i} - \frac{\left[E'_{qi} - X'_{di} I_{di}\right] I_{qi}}{M_i} - \frac{\left[E'_{di} + X'_{qi} I_{qi}\right] I_{di}}{M_i} - \frac{D_i(\omega_i - \omega_s)}{M_i} \ , \tag{5}$$

$$\frac{dE'_{qi}}{dt} = -\frac{E'_{qi}}{T'_{doi}} - \frac{(X_{di} - X'_{di}) I_{di}}{T'_{doi}} + \frac{E_{fdi}}{T'_{doi}} \ , \tag{6}$$

$$\frac{dE'_{di}}{dt} = -\frac{E'_{di}}{T'_{qoi}} + \frac{\left(X_{qi} - X'_{qi}\right) I_{qi}}{T'_{qoi}} \ , \tag{7}$$

$$\frac{dE_{fdi}}{dt} = -\frac{E_{fdi}}{T_{Ai}} + \frac{K_{Ai}}{T_{Ai}}\left(V_{refi} - V_i\right) \ , \tag{8}$$

where: E'_{qi}: Voltage along the quadrature axes of the armature windings,

E'_{di}: Voltage along the direct axes of the armature windings,

I_{di}: Stator current along the direct axis,

I_{qi}: Stator current along the quadrature axis,

X_{di}: Transient reactance along the direct axis,

X'_{di}: Subtransient reactance along the direct axis,

X_{qi}: Transient reactance along the quadrature axis,

X'_{qi}: Subtransient reactance along the quadrature axis,

T'_{doi}: Quadrature axis voltage time constant,

T'_{qoi}: Direct axis voltage time constant,

E_{fdi}: Field voltage,

V_i: Generator terminal voltage,

V_{refi}: Reference voltage of the exciter,

K_{Ai}: Amplifier gain,

T_{Ai}: Amplifier time constant.

We will model the loads as constant impedances; however, the network will be still modeled in full details. The stator algebraic equations are

$$E'_{di} - V_i \sin(\delta_i - \theta_i) - R_{si} I_{di} + X'_{qi} I_{qi} = 0 \,, \tag{9}$$

$$E'_{qi} - V_i \cos(\delta_i - \theta_i) - R_{si} I_{qi} - X'_{di} I_{di} = 0 \quad , \tag{10}$$

and the network algebraic equations

$$\begin{matrix} I_{di} V_i \sin(\delta_i - \theta_i) + I_{qi} V_i \cos(\delta_i - \theta_i) + P_{Li}(V_i) \\ - \sum_{k=1}^{n} V_i V_k Y_{ik} \cos(\theta_i - \theta_k - \alpha_{ik}) = 0 \end{matrix} \,, \tag{11}$$

$$\begin{matrix} I_{di} V_i \cos(\delta_i - \theta_i) - I_{qi} V_i \sin(\delta_i - \theta_i) + Q_{Li}(V_i) \\ - \sum_{k=1}^{n} V_i V_k Y_{ik} \sin(\theta_i - \theta_k - \alpha_{ik}) = 0 \end{matrix} \,, \tag{12}$$

where: $i = 1, \dots, m$,

θ_i: Phase angle of the voltage at bus i,

$P_{Li}(V_i)$: Active power load equation as a function of V_i,

$Q_{Li}(V_i)$: Reactive power load equation as a function of V_i,

Y_{ik}: The magnitude of the admittance between bus *i* and *k*,

α_{ik}: The phase angle of the admittance between bus *i* and *k*.

The complete model for the system will be represented as

$$\begin{aligned} \dot{\underline{x}} &= \underline{f}(\underline{x}), \\ \underline{0} &= \underline{g}\left(\underline{x}, \underline{y}\right), \end{aligned} \tag{13}$$

where: $\underline{x} = (\delta_1, \dots, \delta_m, \omega_1, \dots, \omega_m, E'_{q1}, \dots, E'_{qm}, E'_{d1}, \dots E'_{dm}, E_{fd1}, \dots, E_{fdm})^T$,

$\underline{y} = (I_{d1}, \dots I_{dm}, I_{q1}, \dots I_{qm}, V_1, \dots, V_m, \theta_1, \dots, \theta_m)^T$.

2.2 Brief Review of Power System Stability

Power system stability has been defined by the authors in [7] as *"the ability of an electric power system, for a given initial operating condition, to regain a state of operating equilibrium after being subjected to a physical disturbance, with most system variables bounded so that practically the entire system remains intact"*. They categorized the power system stability problem into three types: rotor angle stability, voltage stability and frequency stability.

Rotor angle stability studies the ability of the synchronous generators in a certain power system to maintain synchronism after a certain disturbance. It is the capability of a power system to restore equilibrium between the mechanical and the electromagnetic torque for each generator. The change of the electromagnetic torque of the synchronous machine after a disturbance can be divided into two parts: the synchronizing torque component and the damping torque component. Both of these components are necessary for the system to get back into stable operating conditions. If the system does not have enough synchronizing torque, the system may go through aperiodic non-oscillatory instability. On the other hand, if the system does not have enough

damping torque, this will result in oscillatory instability. Instability of the power system in these cases can be seen as an increase in the rotor angle of one (or more) generators, resulting in the loss of synchronism with the rest of the system.

The rotor angle stability can time-wise be divided into three types: steady-state, transient, and dynamic [8]. Steady-state stability involves slow or gradual changes in operating points of the system. These studies, which use power flow analysis, guarantee that: 1) Phase angles between system buses are not too large. 2) Bus voltages are close to nominal and 3) Transmission lines, transformers, and other equipment are not overloaded.

Transient stability, the main focus of this work, includes severe disturbances such as loss of generation, line-switching operations, faults, and rapid load changes. Following a disturbance, generators' power angles change, and their frequencies go into temporary deviations from nominal synchronous frequency (60Hz). The objective of a transient stability study is to determine if the machine will return to synchronous frequency with a new steady-state operating point. Changes of power flows and bus voltages are also taken into consideration.

During a transient stability study, the algebraic power-flow equations (representing the network) and the nonlinear differential equations (representing the synchronous machines) are solved. The output of the analysis includes rotor angles and frequencies of synchronous machines, bus voltages, and power flows through lines with the progress of time.

In many cases, transient stability is determined within the first few swings of the machine's rotor angles following a disturbance. During the first few swings, which typically last a few seconds, the mechanical input power and the internal voltage of a generating unit are often assumed constant; they do not change rapidly to have significant impact on the results. However, when the study considers longer swings, models of turbine governors and excitation systems - as well as more detailed machine models - can be employed to obtain accurate transient stability results over longer periods of time.

Dynamic stability involves a longer period than transient stability studies, typically several minutes. It is possible for controllers' actions to affect dynamic stability even if transient stability is preserved. The actions of turbine-governors, excitation systems, tap-changing transformers, and controls from power system operators can interact to stabilize or destabilize a power system several minutes after a disturbance has occurred.

The second type of stability is voltage stability. It is defined as the ability of a power system to preserve nominal voltages at all buses in the system after the disturbance. This stability is characterized by the ability of the power system to restore the equilibrium between load and generation, for both real and reactive powers. Failing to maintain this equilibrium will result in an instability that can be seen as a loss of the load in a certain area, or tripping of some equipment (transmission lines, transformers, etc) by the protective relay system. The sequence of voltage instabilities in the power system can lead to voltage collapse [9, 10]. Voltage collapse is a significant drop in the voltage level of the power system which sometimes can lead to blackouts.

The third and the last type of power system stability is frequency stability. It is the ability of the power system to maintain frequency level after a disturbance that leads to an imbalance between power generation and load, and this has to be done by minimizing any loss of load. Any instability will induce frequency swings which may result in tripping of generators and loads.

2.3 Review of Coherency and Modal Analysis Approaches

In the simulation of power system transient and dynamic stability analysis, a practical approach is to develop simplified power system models. This can help decrease the time and the computational resources required while accurately simulating the system dynamics.

One main objective of a stability investigation is to determine the dynamic response of generators and control systems in a certain area of interest due to disturbances inside that region. However, because of the interconnected nature of power systems, these disturbances will impact the neighboring areas, the so-called external system, which in turn will affect the study region. On the other hand, disturbances in the study region will most likely not excite significantly the internal dynamics of the external system. Thus, a less detailed model of the external system can be used.

Some power system studies, such as contingency analysis and transient stability studies have strict time requirement. Due to these time-consuming studies or the limited computational resources, power engineers usually construct low-order models to represent the power system. They use a fully detailed model for the study area and a reduced model for the external system. The practical method most commonly used by power utilities to derive such reduced models for large power systems is based on the concept of coherency and aggregation of system models. This method uses characteristics of the system in a practical power system to develop a reduced order external system that maintains accurate system dynamics. The characteristics that are usually used are line admittances and loading, machine inertias, and machines rotor angle swings.

Generators that have strong coupling tend to swing together in groups after disturbances, and this characteristic, if used, can help to derive reduced-order models for the system. This phenomenon in a power system is called coherency, which means that some machines experience similar rotor angle swings after a certain disturbance.

The authors in [11] proposed a method using linear time simulation to identify the coherent groups of machines. The method starts by dividing the system into two parts: 1) a study area which is the area of interest where the disturbance will happen and this area needs to be modeled in full details, 2) an external area which is the rest of the power system beside the study area. There is no need to model this area in full detail, and usually a reduced-order model is derived. Modeling of this area is required because it will be affected by the disturbance. However, the disturbance will not have a significant impact on the dynamics and therefore a simplified model is sufficient.

In order to derive a reduced-order model for the external area, the authors rely on identification of coherent groups of generators and then aggregate them. The criterion of coherency is defined as: "two generator buses are coherent if their angular difference is constant within a certain tolerance over a certain time interval". Few assumptions have been made in their study. First, it is assumed that the coherent grouping does not depend on the size of the disturbance. This assumption was verified by observations of different fault strength and noticing that the coherent grouping did not change. Second, the coherent groups do not depend on the model of the generator and its details. It was also observed that the amount of detailing in the model of the generator affects only the damping and has a slight impact on the frequency of the oscillations. This will also be verified in the simulation results of this thesis. Therefore, a classical model for the generators has been used with the governor and the exciter models ignored. Third, the disturbances of the systems have been simulated by injecting mechanical power pulses to the generators as initial conditions.

An additional method for analyzing power system dynamics and the study of coherent generators is the method of slow coherency created by the authors in [12]. The slow coherency idea comes from inter-area modes of oscillation, which is a group of machines swinging together against another group of machines across power system tie-lines. The term 'slow' has been used as the frequency of oscillation for these modes is slower than the frequencies of the local modes that the machines oscillate with against each other in the same group. The phenomenon of inter-area oscillations has been recognized due to the weak coupling through long high impedance tie-lines, or because of highly loaded lines between different areas.

Through singular perturbation method developed by the authors in [13], the system will be demonstrated in the time-scale separation between the inter-area modes and the local modes. Therefore, by using a linearized model for the system, a stiffness coefficient can found which defines the strength of the connection between the machines in the same coherent area. From this coefficient, it is possible to find which machines can be considered as a coherent group, and which are not. The stiffness can be because of the admittance between different areas being smaller than the admittances within the area itself, or due to the number of connection between different areas being less than the number of internal connections. However, sometimes weak connections can be due to both reasons together.

With the aid of the stiffness measure, a linearized system model can be used to find the eigenvalues and the eigenvectors of the system. For power system the dominating modes of oscillation in the swing dynamics are the electromechanical modes, namely the rotor angle and speed. By finding the mode shapes of these modes (eigenvectors components), it is possible to conclude that two machines are slow coherent with respect to a certain inter-area mode if they have similar entries for their corresponding eigenvector components.

One improvement to the previous methods is the hybrid dynamic model developed by the authors in [14]. This hybrid model uses both the conventional coherency approaches discussed earlier and an artificial neural network (ANN) equivalent for model reduction. The neural network equivalent complements the equivalent derived using the coherency-based methods when it comes to the boundary conditions of the study area. As we discussed previously in the conventional coherency approaches, the system equivalent will be divided into two parts: the study area and the external area. The study area boundaries determine the impact on the dynamic behavior of the reduced-order model. The information obtained from one operating point for the initial conditions might not be accurate to describe another operating point, and therefore, when the operating point changes, some errors might be produced. Therefore, the ANN-based equivalent appropriately provides compensation seen as power injections at the boundary buses to preserve the operating conditions. It only uses measurements at the study area boundary buses and can be trained to generate accurate injections at the boundaries, as has been developed in [15]. These measurements replace the detailed model analysis provided by the external area. The

use of the neural network approach by itself has some disadvantages in terms of complexity to capture the full dynamic characteristics of the external area. Therefore this hybrid model has the advantages of both the coherency-based approaches and the neural network approach to find an accurate reduced-order model that is valid for different operating conditions.

Another method has been developed by [16, 17] which utilizes Krylov subspace in addition to a balanced truncation method to find a reduced-order model to power systems without relying on coherency data. This method can be very useful for dealing with large systems, and will yield better results than the methods that rely on eigenvalue calculations. Conventional methods for reduced-order models tend to neglect some behaviors in the power system because they do not have significant effect in the dynamic response. However, this approach focuses on input-output properties of a linear time-invariant system at the boundaries between the study and external areas to get rid of the redundancy in the information, but at the same time maintaining the relations between system inputs and outputs. It can provide an accurate approximation of the original full-detailed model, while representing it by a low-order model.

A modal analysis technique has been developed by the authors in [18] that is used for modeling a power system and for controllers' design. The selective modal analysis (SMA) uses a sensitivity measure defined by the participation factor [10]. The participation factor, from its name, describes how every state variable is participating in a certain mode, and vice versa. It will help identify dynamic patterns associated between the modes and the system states. The SMA finds a set of eigenvalues for a matrix, which is much smaller than the original system matrix, through an iterative process. This method can be used for any linear time-invariant system model, but it has been applied to solve many problems described by small-signal stability and dynamic equivalents for power systems.

It is desirable to develop methods to identify the coherent areas without the extensive eigensubspace computation. The grouping algorithm proposed by the authors in [13] requires the computation of eigenvalues, which can be time consuming for large power systems, despite the availability of sparsity-based techniques to compute a certain number of eigenvalues and eigenvectors. The weak-connection and slow-coherency relationship focuses on exploring weak

connections to find coherent groups. In [19] the authors developed a clustering algorithm based on the state matrix. An incident matrix was derived from the synchronizing torque coefficients and the machine inertias to find weakly connected machine clusters. The identification procedure starts by iteratively computing a coupling factor derived from the synchronizing torque coefficients, through a sequential search of the machines. Then relative changes in the coupling factors define the weakly coherent groups, similar to the slow coherent groups from the grouping algorithm.

It is of basic interest to identify a small number of dominant modes that can approximate the dynamic response that the power system would go through in a certain event, and yield reasonable results. One notion of modal analysis developed in power system is based on small-signal stability dynamics in which we investigate linearized equations of the system model around equilibria. However, since the phenomena of interest will include a lot of nonlinearities when the system is subject to large disturbances and the system might not be in the neighborhood of equilibria anymore, it is questionable whether the global modes for a linearized system are accurate in describing the system undergoing such phenomena. Therefore, there is need to develop a different approach to identify system modes that does not rely on linearization.

In [20], the authors used the Hilbert spectral analysis (HSA) to identify a finite number of time-varying modes from a scalar data obtained with transient stability analysis. The HSA is used to characterize the time evolution of non-stationary power system oscillations after a certain disturbance. This method will rely on data from transient stability measurements to decompose the system into a finite number of time-varying oscillatory components that can be valid for different operating points through the evolution of the system after the disturbance. Certain contingencies in the system can produce large complex interactions in the system that cannot be modeled through a linear approximation. Therefore, it is necessary to include higher order modal approximations through the use of quadratic and cubic nonlinear models to describe the interaction between different frequency components.

In [21], the authors used the proper orthonormal decomposition (POD) to identify a set of dominant components, called PO modes (POMs). These modes are obtained from a subspace

where the bulk of the dynamics of the system occur. The work has been complemented by the authors in [22]. With the aid of the empirical orthogonal function, they were able to describe the energy relationships in the oscillatory components, which made it possible to identify the modes with the most energy. These high energy modes have good accuracy describing the system behavior and they provide valuable information about the level of the non-linear interaction between the modes of oscillation in the system.

Chapter 3 - Koopman Mode Analysis

In this chapter we provide the theory for Koopman mode analysis and the mathematical method for calculating the Koopman modes. In the following section, we discuss Koopman mode applications to power system for coherency identification and the model reduction techniques for power system stability assessment.

3.1 Koopman Modes Theory

The Koopman mode analysis (KMA) is a modal decomposition for nonlinear dynamics based on spectral analysis of a linear operator, called the Koopman operator. This operator is defined for any system, linear or nonlinear. Even if the observed dynamic system elements are finite dimensional, the Koopman operator is infinite dimensional, and does not rely on linearization of the dynamics. This method is an alternative method for identification of modes and coherency, by analysis of short-term swing dynamics in multi-machine power systems. The authors showed in [23] via spectral analysis of the Koopman operator that single-frequency modes can be embedded in highly nonlinear spatiotemporal dynamics, which they called the Koopman modes. Computation of the KMs is applicable to dynamics of any power system and can be performed on finite-time data of the dynamics. Therefore, the KMA is suitable for analysis of both simulation outputs and measured data in practical systems. This analysis will have two outcomes. First, these modes will be used to identify single-frequency, spatial modes embedded in coupled swing dynamics of the machines. Second, the KMA will be used to identify coherency groups of machines, and as a stability measure for power system dynamics. The following theoretical analysis is based on [24-26].

Considering a continuous-time system governed by the differential equation as:

$$\underline{\dot{x}} = \underline{f}(\underline{x}(t)) \,, \tag{14}$$

where $\underline{f}$ is a nonlinear function. However, we are interested in discrete data. To represent our equation for discrete time, we define $\underline{\Phi}_0^{\mathrm{h}}$ as the state transition function for a finite time-h mapping. Therefore, the states of our system will be defined as follows:

$$\begin{aligned} x[k] &= x(t_k) \text{ and } h = t_{k+1} - t_k \\ \underline{x}[k+1] &= \underline{\Phi}_0^{\mathrm{h}}(\underline{x}[k]) \, . \end{aligned} \tag{15}$$

We apply now the Koopman operator on the discrete-time system. The Koopman operator is a linear operator *U* that acts on a scalar-valued function to map it into a new function given by

$$U\underline{p}(\underline{x}) = \underline{p} \text{ o } \underline{\Phi}_0^{\mathrm{h}}(\underline{x}) \, , \tag{16}$$

Even though the discrete-time system can be given as a non-linear function, the Koopman operator is linear, but infinite dimensional. The eigenfunctions and eigenvalues of U are defined as:

$$U\varphi_i(\underline{x}) = \lambda_i \varphi_i(\underline{x}) \, , \qquad \text{for } \; i = 1, 2, \ldots \tag{17}$$

for scalar-valued functions φ_i and constants λ_i.

If $\underline{x}$ contains the full information about the dynamics at an instance of time, we define a vector-valued observable $\underline{p}(\underline{x})$ which is a vector of any variable of interest, such as rotor angles, speeds, voltages, … . Using the Koopman operator, the authors in [23] showed that if the initial condition $\underline{x}_o$ is on-attractor, then $\underline{p}(\underline{x})$ can be exactly represented as follows:

$$\underline{p}(\underline{x}) = \sum_{j=1}^{\infty} \varphi_j(\underline{x}) \underline{v}_j + \begin{bmatrix} \int_0^{2\pi} e^{i\theta} dE(\theta) p_1(\underline{x}) \\ \vdots \\ \int_0^{2\pi} e^{i\theta} dE(\theta) p_\mu(\underline{x}) \end{bmatrix}, \tag{18}$$

where μ is the number of observables.

The function $E(\theta)$ is a continuous, complex spectral measure. The first term of the right-hand side, represents the contribution of the discrete spectra of *U* and describes the quasi-periodic behavior in the time evolution of the observable. Alternatively, the other term describe the aperiodic behavior of $\underline{p}(\underline{x})$.

Practical experience suggests that dynamics observed of a power system does not have continuous spectrum in the frequency domain, and conversely shows a finite number of discrete spectra in the frequency domain. Therefore, by neglecting the continuous spectrum part of *U*, the dynamics can be represented as

$$\underline{p}(\underline{x}) = \sum_{j=1}^{\infty} \varphi_j(\underline{x})\underline{v}_j \tag{19}$$

The functions φ_j will be referred to as Koopman eigenfunctions and λ_j as Koopman eigenvalues.

We will think of the expression as expanding the function $\underline{p}(\underline{x})$ as a linear combination of the eigenfunctions $\varphi_i(\underline{x})$ of U, and $\underline{v}_j$ are the vector coefficients in the expansion. The vectors $\underline{v}_j$ are referred to as Koopman modes. Iterating from $\underline{x}_o$, (19) can be given by

$$\underline{p}(\underline{x}[k]) = \sum_{j=1}^{\infty} U^k \varphi_j(\underline{x}_o)\underline{v}_j = \sum_{j=1}^{\infty} \lambda_j^k \varphi_j(\underline{x}_o)\underline{v}_j. \tag{19}$$

For a system evolving on-attractor, the Koopman eigenvalues always lie on the unit circle. However, for dynamics off-attractor, the Koopman eigenvalues λ_j characterize the temporal behavior of the corresponding Koopman mode $\underline{v}_j$: the phase of λ_j determines its frequency and the magnitude determines the growth rate.

For example let's apply Koopman mode analysis on linear systems, which is generated by a linear mapping function f given by the following equation:

$$f(\underline{x}) = \underline{A}\,\underline{x}. \tag{20}$$

It can be proven that the eigenvalues of A are the same eigenvalues of U, and the eigenvectors of A are related to the eigenvectors of U as well. Let $\lambda_j$and υ_j represent the eigenvalues and eigenvectors of A, respectively. Then we have the following:

$$\underline{A}\underline{\upsilon}_j = \lambda_j \underline{\upsilon}_j \ , \qquad \text{for } j = 1, \dots, n. \tag{21}$$

Let w_j be the eigenvectors defined for the adjoint A^* such that $\underline{A}^* \underline{w}_j = \lambda_j \underline{w}_j$

Next we define scalar-valued function

$$\varphi_j(\underline{x}) = < \underline{x}, \underline{w}_j > \ , \qquad \text{for } \ j = 1, \dots, n \tag{22}$$

where $< \cdot, \cdot >$ denotes the inner product of the two vectors.

Then by applying the linear operator, *U*, in (20) we obtain:

$$U\varphi_j(\underline{x}) = \varphi_j(\underline{A}\,\underline{x}). \tag{23}$$

Taking into consideration (21), and the property (22) we derive respectively (24) and (25).

$$U\varphi_j(\underline{x}) \ = < \underline{x}, \underline{A}^* \, \underline{w}_j > \tag{24}$$

$$U\varphi_j(\underline{x}) = \lambda_j < \underline{x}, \underline{w}_j > = \ \lambda_j \varphi_j(\underline{x}) \, . \tag{25}$$

We can conclude that $\varphi_i(x)$ are the eigenfunctions of U, with eigenvalues λ_j.

Now we can write the following:

$$\underline{x} = \sum_{j=1}^{n} < \underline{x}, \underline{w}_j > \underline{\upsilon}_j = \sum_{j=1}^{n} \varphi_j(\underline{x}) \, \underline{\upsilon}_j \ , \tag{26}$$

which demonstrates that for linear systems, the Koopman modes coincide with the eigenvectors of *A*.

3.2 Computation of Koopman Modes

We will assume that for any state $\underline{x}$, we can measure a vector-valued observables $\underline{p}(\underline{x})$. The method used is the Arnoldi method which is commonly used for linear systems. We show that when the aforementioned method is applied to nonlinear systems, it will actually produce approximations to the eigenvalues of the Koopman operator, and their corresponding modes.

For a linear system defined as

$$\underline{x}_{k+1} = \underline{A}\,\underline{x}_k, \tag{27}$$

where x has dimension n, and n is so large that we cannot compute the eigenvalues of A directly.

A common method for computing estimates of the eigenvalues is the Krylov method. The method starts by computing iterates from an initial vector $\underline{x}_o$. After $m-1$ iterations, we will obtain a group of m vectors that span the Krylov subspace spanned by $\{\underline{x}_o, \underline{A}\underline{x}_o, \underline{A}^2\underline{x}_o, \dots., \underline{A}^{m-1}\underline{x}_o\}$. We then find an approximation for the eigenvalues and eigenvectors by projecting A onto the low-ranked m-dimensional subspace. If we build the vectors from the subspace into a n x m matrix we get

$$\begin{aligned}\underline{K} &= \left[\underline{x}_o, \underline{A}\underline{x}_o, \underline{A}^2\underline{x}_o, \dots., \underline{A}^{m-1}\underline{x}_o\right] \\ &= \left[\underline{x}_o, \underline{x}_1, \dots, \underline{x}_{m-1}\right].\end{aligned} \tag{28}$$

We will now consider two cases. The first one is a special case where the m^{th} iterate is a linear combination of the previous vectors, can be written as

$$\begin{aligned}\underline{x}_m &= \underline{A}\,\underline{x}_{m-1} \\ &= c_o\underline{x}_o + c_1\underline{x}_1 + \cdots + c_{m-1}\underline{x}_{m-1} = \underline{K}\,\underline{c}\ \ ,\end{aligned} \tag{29}$$

where $\underline{c} = (c_o, c_1, \dots, c_{m-1})^T$,

Then we have

$$\underline{A}\,\underline{K} = \underline{K}\,\underline{C}\,, \tag{30}$$

where C is called a companion matrix given by

$$\underline{C} = \begin{bmatrix} 0 & 0 & & 0 & c_o \\ 1 & 0 & \cdots & 0 & c_1 \\ 0 & 1 & & 0 & c_2 \\ \vdots & & \ddots & & \vdots \\ 0 & 0 & \cdots & 1 & c_{m-1} \end{bmatrix}\,, \tag{31}$$

We find can write the Companion matrix using its eigenvalues and eigenvectors as follows:

$$\underline{C} = \underline{T}^{-1}\underline{\Lambda}\,\underline{T}\ , \tag{32}$$

where the eigenvectors are the columns of $\underline{T}^{-1}$and the eigenvalues are the diagonal entries of the matrix $\underline{\boldsymbol{\Lambda}}$. We define $\underline{v}$ as the columns of $\underline{V} = \underline{K}\,\underline{T}^{-1}$.

It was shown in [27] that the eigenvalues of C are a subset of the eigenvalues of A. It can also be verified that $\underline{v} = \underline{Ka}$ is an eigenvector of A, with eigenvalue λ, where $\underline{a}$ is defined as

$$\underline{Ca} = \lambda\underline{a}\ , \tag{33}$$

The second case which is the general case - when the m^{th} iterate is not a linear combination of the previous iterates, we have a residual instead of the equality, defined as

$$\underline{r} = \underline{x}_m - \underline{K}\,\underline{c}\,. \tag{34}$$

This residual can be minimized by choosing c accordingly to yield $\underline{r}$ to be orthogonal to the span $\{\underline{x}_o, \underline{x}_1, \dots, \underline{x}_{m-1}\}$. The eigenvalues in this case are approximations to the eigenvalues of A, called Ritz values, and the corresponding approximate eigenvectors are given by $\underline{v} = \underline{Ka}$, called Ritz vectors.

An important feature of the method that it does not require explicit knowledge of the matrix A. All it requires is a sequence of vectors $\{\underline{x}_o, \underline{x}_1, \dots, \underline{x}_{m-1}\}$ obtained from the observables of the system.

Now for the case of a nonlinear system, considering a set of data $\{\underline{x}_o, \underline{x}_1, \dots, \underline{x}_{m-1}\}$, and let $\tilde{\lambda}_j$, $\underline{\tilde{v}}_j$ be the empirical Ritz values and vectors of this sequence. Then

$$\underline{x}_k = \sum_{j=1}^{m} \lambda_j^k \underline{v}_j \ , \qquad \text{for } k = 0, .., m-1 \tag{35}$$

$$\underline{x}_m = \sum_{j=1}^{m} \lambda_j^m \underline{v}_j + \underline{r} \ , \tag{37}$$

$$\underline{r} \perp span\{\underline{x}_o, \underline{x}_1, \dots, \underline{x}_{m-1}\}.$$

We can write $\underline{K}$ as following:

$$\underline{K} = [\underline{x}_o \ \ \underline{x}_1 \ \cdots \ \underline{x}_{m-1}] = [\underline{v}_1 \ \underline{v}_2 \cdots \underline{v}_m] \begin{bmatrix} 1 & \lambda_1 & \lambda_1^2 & \cdots & \lambda_1^{m-1} \\ 1 & \lambda_2 & \lambda_2^2 & & \lambda_2^{m-1} \\ & \vdots & & \ddots & \vdots \\ 1 & \lambda_m & \lambda_m^2 & \cdots & \lambda_m^{m-1} \end{bmatrix}$$

$$\underline{K} = \underline{V}\,\tilde{\underline{T}}. \tag{36}$$

The rightmost matrix is the Vandermonde matrix, which diagonalizes the companion matrix $\underline{C}$ defined in (32) as long as the eigenvalues are distinct. That means $\tilde{T}$ is exactly matrix T in (33), and therefore, $\underline{K} = \underline{V}\,\tilde{\underline{T}}$.

Comparing the expansion of (20) with $[(\underline{x}_k)]$ in (36), we can see that the empirical Ritz values $\tilde{\lambda}_j$, and vectors $\underline{\tilde{v}}_j$ behave similar to the eigenvalues $\lambda_j$and modes $\underline{v}_j$ of U, but for a finite sum instead of an infinite one.

If $\underline{r} = \underline{0}$, then as far as the data is concerned, the approximate modes are indistinguishable from the true eigenvalues and Koopman modes of U, with an expansion consisting of a finite number

of terms. If $\underline{r} \neq \underline{0}$, then the values $\tilde{\lambda}_j$ are approximations of the true eigenvalues λ_j of U, and the eigenvectors $\underline{\tilde{v}}_j$ are approximations of the Koopman modes $\underline{v}_j$ with a scaling factor of $\varphi_j(\underline{x}_o)$.

3.3 Koopman Modes Applications to Power Systems

3.3.1 Coherency Identification

Using the results from Koopman modes analysis, it is possible to identify coherent grouping of machines. We can say that a group of machines $I = \{1, \dots, p\}$ is coherent with respect to mode j, if the j^{th} Koopman mode components are equal for all $i \in I$. Then for coherent identification for mode j, it is sufficient to check both the amplitude and the angles for the corresponding Koopman mode components [10]. Numerically, it is enough to group machines with similar (not exactly equal) Koopman mode components, as a set of coherent machines. The Koopman mode components describe the behavior of each machine with respect to the frequency of oscillation. Therefore, it can be considered that the machines with similar entries for the KM are experiencing similar behaviors, and as a result, they are coherent with respect to that mode.

3.3.2 Precursor to Coherent Swing Instabilities

The purpose is to identify a precursor to swing instabilities in short-term dynamics by using numerical simulation, in addition to mathematical models, so system operators can monitor, analyze, and control the phenomena of interest. The loss of transient stability of power system is associated with non-local dynamics of a power system, in the sense that it does not happen upon an infinitesimal perturbation around an equilibrium operating point of the system. It compasses the situation when the system escapes it predefined set around the equilibrium.

This analysis provides a precursor to one type of loss of transient stability, coherent swing instability (CSI) described by the authors in [28]. CSI is an emergent and undesirable phenomenon of synchronous machines in power system, in which a group of machines in the system coherently loses synchronism with the rest of the system after being subject to a finite local disturbance. The dynamical mechanism of CSI explains how local plant mode oscillations, inter-area mode instability, and multi-swing instability interact to destabilize the system.
The precursor is an emergent path of energy from high KMs to the lowest with flat basis vector [26], which is termed the coherent KM. The precursor to the instability can be seen as an unstable mode which will grow largely and eventually diverge and destabilize the system.

Practical experience suggest that the dynamics of power systems have a finite number of clean peaks in the frequency spectrum, that is can be represented with a finite number of oscillatory modes. A relevant mathematical model is the dynamical system with a finite number N of oscillatory modes, described by

$$\begin{aligned} \frac{dr_i}{dt} &= h_i(r_1, \dots, r_N, \theta_1, \dots, \theta_N), \\ \frac{d\theta_i}{dt} &= \Omega_{\mathrm{i}} + q_i(r_1, \dots, r_N, \theta_1, \dots, \theta_N), \end{aligned} \tag{37}$$

where $i = 1, \dots, N$ denotes the number of modes, r_i the amplitude of the oscillatory mode i, θ_i its rotating phase, and Ω_{i} its angular frequency. The functions h_i and q_i define the interaction between different modes. Since the dynamical system in the model is nonlinear, different initial conditions possibly induce different asymptotic behaviors. We may find for one or some modes, the amplitudes grow in an unbounded way. This corresponds to the development of oscillatory instabilities following a large but finite local disturbance.

However, we need to include model reduction based on KM and the Galerkin projection approximation, the action-angle representation, to convert the original system model represented by observable states into a reduced order model represented by a handful of Koopman modes.
We approximate the original dynamical system model by projecting the dynamics onto a low-dimensional subspace spanned by a number of KMs. This will provide a reduced-order model.

We will use $\varphi_i = \varphi_i(x_o)v_i$, and view λ_i^k as a time-dependent variable $z_i[k]$. Using the KMs calculated for m samples, we can express the observable as

$$\underline{p}(\underline{x}_k) = \sum_{j=1}^{\infty} z_i[k]\underline{\varphi}_j,$$
$$\underline{p}(\underline{x}_k) \cong \sum_{j=1}^{m} z_i[k]\underline{\varphi}_j = \underline{\mathcal{V}}\,\underline{Z}[k] \ , \tag{38}$$

where $\underline{\mathcal{V}} = (\underline{\varphi}_1, \dots, \underline{\varphi}_m)$ with dimension of pxm, and $\underline{Z} = (z_1, \dots z_m)^T$ with dimension of mxm. By substituting (40) in (15), we can write (15) as

$$\sum_{i=1}^{m} z_i[k+1]\underline{\varphi}_i = \left(\underline{p}\ o\ \underline{\Phi}_0^{\mathrm{h}}\ o\ \underline{p}^{-1}\right)\left(\underline{\mathcal{V}}\,\underline{Z}[k]\right) \ , \tag{39}$$

Multiplying both sides by $\underline{\varphi}_j^*$, we have

$$\sum_{i=1}^{m} z_i[k+1]\underline{\varphi}_j^*\underline{\varphi}_i = \underline{\varphi}_j^*\left(\underline{p}\ o\ \underline{\Phi}_0^{\mathrm{h}}\ o\ \underline{p}^{-1}\right)\left(\underline{\mathcal{V}}\,\underline{Z}[k]\right) = \underline{T}_j(\underline{Z}[k]) \ , \tag{40}$$

where $j = 1, \dots, m$ and can also be written as

$$\underline{E}\,\underline{Z}[k+1] = \underline{T}\left(\underline{Z}[k]\right) \ , \tag{41}$$

where $\underline{E} = \underline{\mathcal{V}}^*\underline{\mathcal{V}}$ with dimension of mxm, and $\underline{T}(\underline{Z}) = (\underline{T}_1(\underline{Z}), \dots, \underline{T}_m(\underline{Z}))^T$ with dimension of mxm.

This gives us a discrete-time reduced-order system of (15) in terms of the first m KMs. This reduction is a combination of measured data to compute KMs and of a mathematical model. Now we introduce the action-angle variables for the reduced-order system. By defining $z_j = r_j\, e^{\mathrm{i}\theta_j}$, where r and θ are both positive real numbers, we rewrite (43) as

$$r_j[k+1]e^{\mathrm{i}\theta_j[k+1]} = P_j\left(\underline{r}[k], \underline{\theta}[k]\right) \ , \tag{42}$$

where $\underline{r} = (r_1, \dots, r_m)^T$, and $\underline{\theta} = (\theta_1, \dots, \theta_m)^T$,

$$P_j(r,\theta) = \sum_{i=1}^{m} \left[\underline{E}^{-1}\right]_{ji} T_i(r_1\, e^{\mathrm{i}\theta_1}, \ldots, r_m\, e^{\mathrm{i}\theta_m})\ . \tag{43}$$

We can then rewrite (44) as

$$r_j[k+1] = \left|P_j\left(\underline{r}[k], \underline{\theta}[k]\right)\right| = \underline{F_j}\left(\underline{r}[k], \underline{\theta}[k]\right)\ , \tag{44}$$

$$\theta_j[k+1] = Arg(P_j\left(\underline{r}[k], \underline{\theta}[k]\right)) = \underline{G_j}\left(\underline{r}[k], \underline{\theta}[k]\right)\ , \tag{45}$$

$$\begin{aligned} \underline{r}[k+1] &= \underline{F}\left(\underline{r}[k], \underline{\theta}[k]\right), \\ \underline{\theta}[k+1] &= \underline{G}\left(\underline{r}[k], \underline{\theta}[k]\right), \end{aligned} \tag{46}$$

The system in (48) is the reduced-order model that will be used for developing a precursor to the system instability.

Chapter 4 - Case studies

In this chapter, we apply the Koopman mode analysis on two test systems. The first test system is the 2-area 4-machine system[10], which is used to compare the modes obtained from the KMA with those derived by linearization around the equilibrium. The second test system is the IEEE 10-machine 39-bus system, which is used to show the coherency identification method and the precursor to system instability.

4.1 Four-Machine Two-Area System

We make a comparison between small-signal stability analysis [6, 10], and Koopman mode analysis in terms of modal analysis and coherency identification. The test system shown in Figure 1 is the four-machine two-area system, and its data can be found in [6]. We use the two-axis model for generators developed in chapter 2.

4.1.1 Koopman Modes Analysis for Four-Machine Two-Area System

We first use Koopman modes to analyze the system. This will be done by disturbing the system with a fault with duration of $230\,ms$ at bus 13, then subsequently clearing the fault without modifying the network topology. The dynamic simulation results are shown in Figure 2.

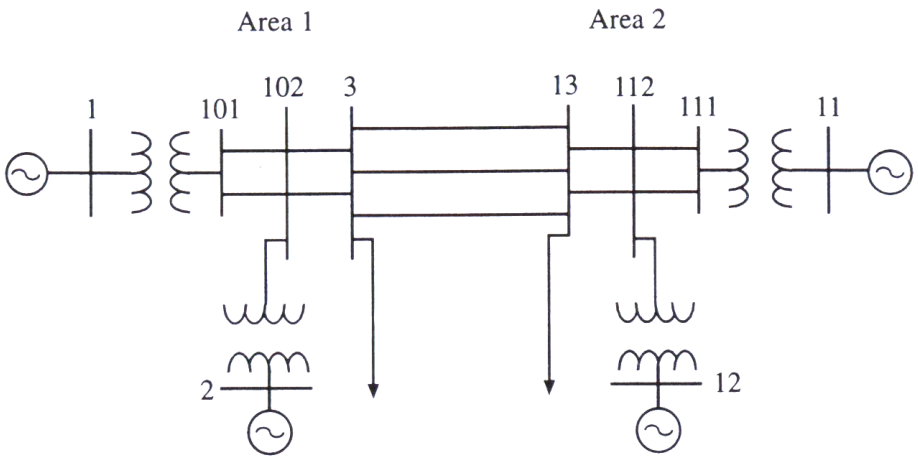

Figure 1: 2-area 4-machine system diagram. P. W. Sauer and M. Pai, *Power system dynamics and stability* vol. 6: Prentice Hall Upper Saddle River, NJ, 1998. Used under fair use, 2014.

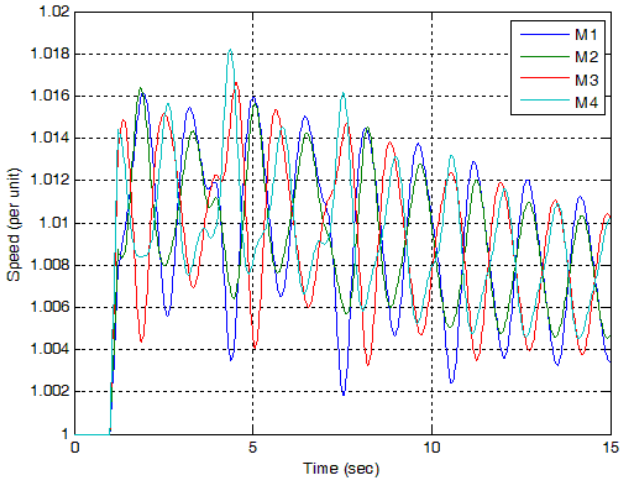

Figure 2: Simulation Results, Rotor speeds with respect to time

From these observables, we can build a Krylov subspace represented by

$$\underline{K} = [\underline{p}(\underline{x}_o), \underline{p}(\underline{x}_1), \dots, \underline{p}(\underline{x}_m)].$$

The number of samples monitored in this case are ($m = 750$), and the observables, $\underline{p}(\underline{x})$, are

$$\underline{p}(\underline{x}) = (V_{t1}, \dots, V_{t4}, \delta_1, \dots, \delta_4, E_{fd1}, \dots, E_{fd4}, I_{t1}, \dots, I_{t4}, \omega_1, \dots, \omega_4)^T,$$

where: V_{ti}: Generator terminal voltage (in per unit),

δ_i: Generator rotor angle (in rad),

E_{fdi}: Excitation field voltage (in per unit),

I_{ti}: Stator current (in per unit),

ω_i: Generator speed (in per unit).

To build the companion matrix, we need to choose the coefficients $\underline{c} = (c_o, \dots, c_{m-1})^T$, that minimize the residual $\underline{r} = \underline{x}_m - \underline{K}\underline{c}$. Because $\underline{r}$ is perpendicular to the span $\{\underline{p}(\underline{x}_o), \underline{p}(\underline{x}_1), \dots, \underline{p}(\underline{x}_{m-1})\}$, we can rewrite (37) as

$$0 = \underline{p}(\underline{x}_i)^T \underline{r} = \underline{p}(\underline{x}_i)^T \underline{p}(\underline{x}_m) - \sum_{j=0}^{m-1} c_i \underline{p}(\underline{x}_i)^T \underline{p}(\underline{x}_j) , \quad (47)$$

where $i = 0, \dots, m-1$.

We define $\underline{A} = \{A_{ij}\}$ as

$$A_{ij} = \underline{p}(\underline{x}_i)^T \underline{p}(\underline{x}_j) . \quad (48)$$

Because A has at most rank of $20 < m$, it is not possible to determine a unique minimize $\underline{c}$ of the norm $||\underline{A}\,\underline{c} - \underline{b}||$ where $\underline{b} = \underline{p}(\underline{x}_i)^T \underline{p}(\underline{x}_m)$. Therefore, we can minimize the norm using the pseudo-inverse matrix $\underline{A}^\dagger$ of $\underline{A}$. Then $\underline{c}$ can be found by

$$\underline{c} = \underline{A}^\dagger \underline{b}. \quad (49)$$

Now, we can find the companion matrix defined in (32), and from which we can find its eigenvalues, defined as the Ritz eigenvalues $\tilde{\lambda}_1, \dots, \tilde{\lambda}_m$. To find the associated eigenvectors $\tilde{v}_1, \dots, \tilde{v}_m$, we can either use the eigenvectors of the companion matrix or the Vandermonde matrix $\underline{\tilde{T}}$ defined in (33). We can then project this vector space through the Krylov subspace to get the Ritz eigenvectors. Here we will use the Vandermonde matrix to find the Ritz eigenvectors as

$$\underline{V} = \underline{K}\,\underline{T}^{-1} , \quad (50)$$

Now we have the full set of Ritz eigenvalues $\tilde{\lambda}$, and Ritz eigenvectors $\tilde{v}$. We select a small group of the available modes by choosing the ones with the largest growth rate and norm. The chosen modes according to these criteria are shown in Table 1. We can also check if the analysis has captured the dominant frequencies by applying DFT on the observables (rotor angles and speeds) obtained from the simulations. The results of the DFT are shown in Figure 3. We can see that the modes with frequencies 0.65, 0.99 and 1.3 Hz have been identified by KMA and showing dominancy as they have high growth rates and norms.

Table 1: Modes eigenvalues, frequencies, growth rate and norms

No.	Eigenvalue	Frequency	Growth rate	Norm
1	0.9845 ∓ 0.1633i	1.308	0.9980	5.038
2	0.9895 ∓ 0.1241i	0.9927	0.9972	10.68
3	0.9908 ∓ 0.1127i	0.9011	0.9972	10.57
4	0.9907 ∓ 0.1032i	0.8263	0.9960	7.758
5	0.9930 ∓ 0.0929i	0.7421	0.9973	13.75
6	0.9955 ∓ 0.0211i	0.1687	0.9957	2.800
7	0.9957 ∓ 0.0820i	0.6541	0.9991	41.43
8	0.9961 ∓ 0.0080i	0.0639	0.9960	4.527
9	0.9939 ∓ 0.0589i	0.4710	0.9956	4.243
10	0.9935 ∓ 0.0698i	0.5583	0.9959	14.23

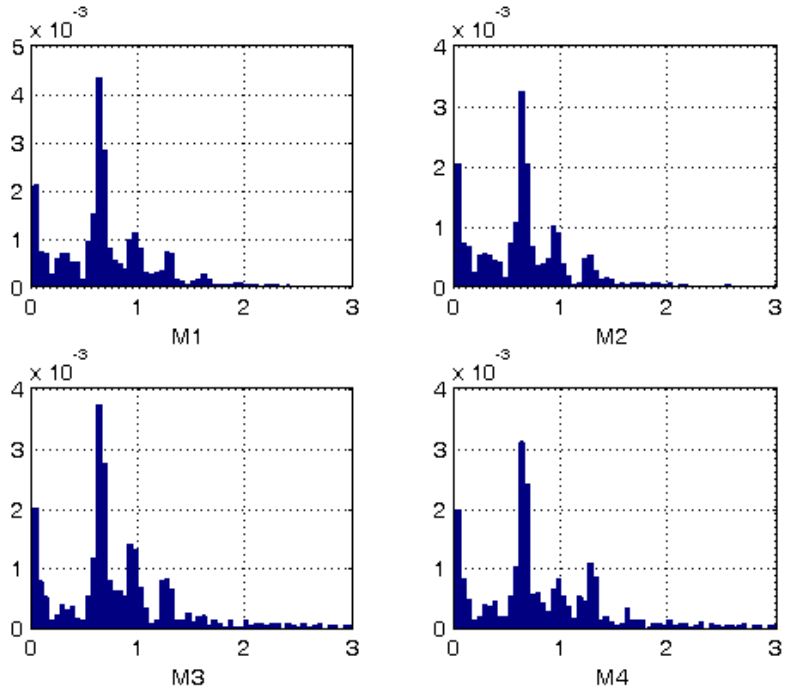

Figure 3: Discrete Fourier Transform for rotor angle speeds

In order to categorize the modes as local or interarea, we will use the criterion described in [19]. By plotting the Ritz eigenvectors for each mode on the phasor plane, shown in Figures 4 and 5, we can notice that machines (1,2) and (3,4) are expressing similar behavior with respect to mode 7 and 9 . It can be considered as machines (1,2) are swinging together against machines (3,4). Therefore, modes 7 and 9 will be considered interarea modes, with machines (1,2) and machines (3,4) forming two coherent groups with respect to these modes. On the other hand, by noticing the mode shape for mode 1 in Figure 6 we can see that machines (3) and (4) have larger corresponding amplitudes of the Ritz eigenvector component. Also, these machines are showing similar amplitudes and opposite directions. Then, it can be considered as machines (3) and (4) are swinging against each other with respect to mode 1. Therefore, mode 1 will be considered as a local mode. In a similar way we can categorize the rest of the modes as interarea or local modes.

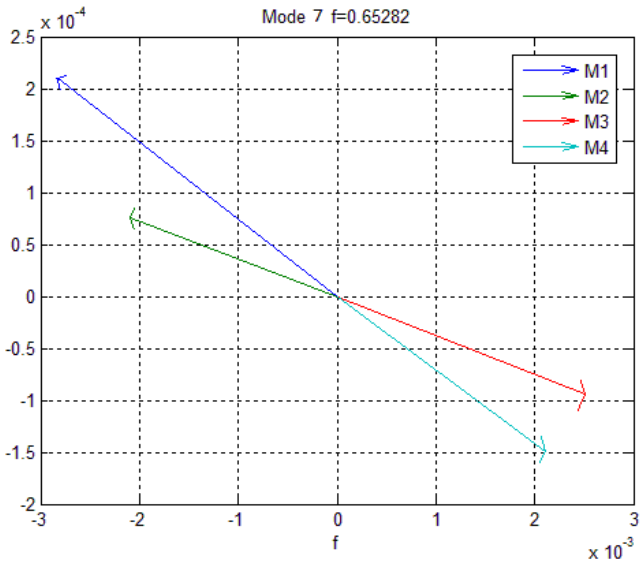

Figure 4: Mode shape for mode 7

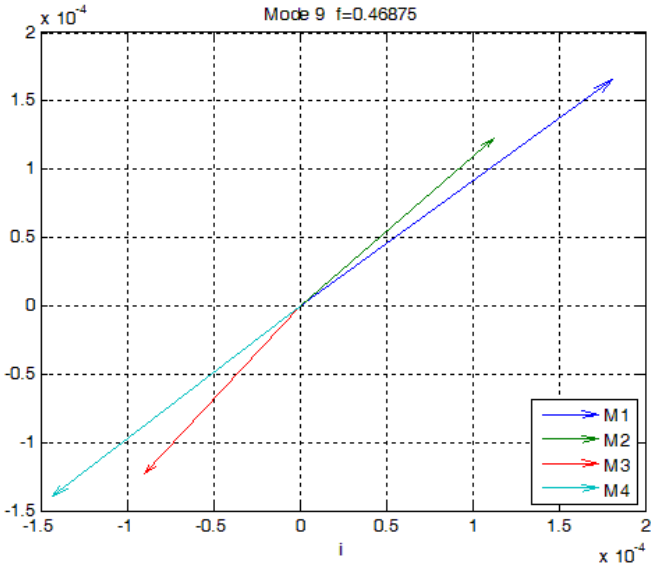

Figure 5: Mode shape for mode 9

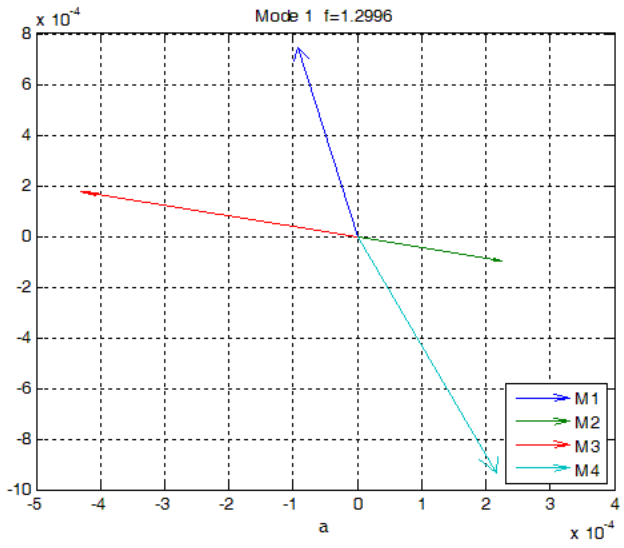

Figure 6: Mode shape for mode 6

4.1.2 Small Signal Stability Analysis for Four-Machine Two-Area System

Now we will analyze the system using the small-signal stability method. The small-signal analysis is based on studying system stability under small disturbances, that the system model can be linearized around the equilibrium point. This can provide valuable information about the inherent dynamic characteristics of the power system and help in the design of controllers.

Following the analysis in [6], the system model, represented by the machines generators differential equations (4)-(8) and the stator and network algebraic equations (9)-(12), can be linearized around the equilibrium point as following

$$\frac{d\Delta\delta_i}{dt} = \Delta\omega_i \ , \tag{51}$$

$$\begin{aligned}\frac{d\Delta\omega_i}{dt} = \frac{\Delta T_{Mi}}{M_i} - \frac{E'_{qio}\Delta I_{qi}}{M_i} + \frac{X'_{dio}I_{dio}\Delta I_{qi}}{M_i} + \frac{X'_{di}I_{qio}\Delta I_{di}}{M_i} - \frac{I_{qio}\Delta E'_{qi}}{M_i} \\ - \frac{E'_{dio}\Delta I_{dio}}{M_i} - \frac{I_{dio}\Delta E'_{di}}{M_i} - \frac{X'_{qi}I_{dio}\Delta I_{qi}}{M_i} - \frac{X'_{qi}I_{qio}\Delta I_{di}}{M_i} - \frac{D_i}{M_i}\Delta\omega_i,\end{aligned} \tag{52}$$

$$\frac{d\Delta E'_{qi}}{dt} = -\frac{\Delta E'_{qi}}{T'_{doi}} - \frac{(X_{di}-X'_{di})\Delta I_{di}}{T'_{doi}} + \frac{\Delta E_{fdi}}{T'_{doi}} \ , \tag{53}$$

$$\frac{d\Delta E'_{di}}{dt} = -\frac{\Delta E'_d}{T'_{qoi}} + \frac{(X_q - X'_q)\Delta I_{qi}}{T'_{qoi}}, \tag{54}$$

$$\frac{d\Delta E_{fdi}}{dt} = -\frac{\Delta E_{fdi}}{T_{Ai}} + \frac{K_{Ai}}{T_{Ai}}\left(\Delta V_{refi} - \Delta V_i\right), \tag{55}$$

for $i = 1, \ldots, 4$

which can be written in matrix form for all machines as

$$\Delta\dot{\underline{x}} = \underline{A}_1\Delta\underline{x} + \underline{B}_1\Delta\underline{I}_g + \underline{B}_2\Delta\underline{V}_g + \underline{E}_1\Delta\underline{U}\ , \tag{56}$$

where $\underline{A}_1, \underline{B}_1, \underline{B}_2, \underline{E}_1$ are diagonal matrices, and

$$\underline{x} = \left[\underline{x}_1^t \ldots \underline{x}_m^t\right]^T,$$
$$\underline{x}_i = \left[\delta_i\ \omega_i\ E'_{qi}\ E'_{di} E_{fdi}\right]^T,$$
$$\underline{I}_g = \left[I_{d1} I_{q1} \ldots I_{dm} I_{qm}\right]^T,$$
$$\underline{V}_g = \left[\theta_1 V_1 \ldots \theta_m V_m\right]^T.$$

For the stator equations (9) and (10), the linearized equation can be written as

$$\begin{aligned}\Delta E'_{di} - \sin(\delta_{io} - \theta_{io})\,\Delta V_i - V_{io}\sin(\delta_{io} - \theta_{io})\,\Delta\delta_i \\ + V_{io}\cos(\delta_{io} - \theta_{io})\,\Delta\theta_i - R_{si}\Delta I_{di} + X'_{qi}\Delta I_{qi} = 0\ ,\end{aligned} \tag{57}$$

$$\begin{aligned}E'_{qi} - \cos(\delta_{io} - \theta_{io})\,\Delta V_i + V_{io}\sin(\delta_{io} - \theta_{io})\,\Delta\delta_i \\ - V_{io}\sin(\delta_{io} - \theta_{io})\,\Delta\theta_i - R_{si}\Delta I_{qi} - X'_{di}\Delta I_{di} = 0\ ,\end{aligned} \tag{58}$$

Therefore, the stator equations for all machines can be written as

$$\underline{0} = \underline{C}_1\Delta\underline{x} + \underline{D}_1\Delta\underline{I}_g + \underline{D}_2\Delta\underline{V}_g, \tag{59}$$

where $\underline{C}_1, \underline{D}_1, \underline{D}_2$ are block diagonal matrices.

For the generator buses network equations (11) and (12), the linearized equations are given by:

$$V_{io}\sin(\delta_{io}-\theta_{io})\,\Delta I_{dio}+I_{dio}\sin(\delta_{io}-\theta_{io})\,\Delta V_i+I_{dio}V_{io}\cos(\delta_{io}-\theta_{io})\,\Delta\delta_i$$
$$-I_{dio}V_{io}\cos(\delta_{io}-\theta_{io})\,\Delta\theta_i+V_{io}\cos(\delta_{io}-\theta_{io})\,\Delta I_{qi}+I_{qio}\cos(\delta_{io}-\theta_{io})\,\Delta V_i$$
$$-I_{qio}V_{io}\sin(\delta_{io}-\theta_{io})\,\Delta\delta_i+I_{qio}V_{io}\sin(\delta_{io}-\theta_{io})\,\Delta\theta_i-\left[\sum_{k=1}^{n}V_{ko}Y_{ik}\cos(\theta_{io}-\theta_{ko}-\alpha_{ik})\right]\Delta V_i$$
$$-V_{io}\sum_{k=1}^{n}[Y_{ik}\cos(\theta_{io}-\theta_{ko}-\alpha_{ik})]\Delta V_k+\left[V_{io}\sum_{k=1,\neq i}^{n}V_{ko}Y_{ik}\sin(\theta_{io}-\theta_{ko}-\alpha_{ik})\right]\Delta\theta_i$$
$$-V_{io}\textstyle\sum_{k=1,\neq i}^{n}[V_{ko}Y_{ik}\sin(\theta_{io}-\theta_{ko}-\alpha_{ik})]\,\Delta\theta_k+\frac{\partial P_{li}(V_i)}{\partial V_i}\Delta V_i=0\quad,\qquad(60)$$

$$V_{io}\cos(\delta_{io}-\theta_{io})\,\Delta I_{dio}+I_{dio}\cos(\delta_{io}-\theta_{io})\,\Delta V_i+I_{dio}V_{io}\sin(\delta_{io}-\theta_{io})\,\Delta\delta_i$$
$$+I_{dio}V_{io}\sin(\delta_{io}-\theta_{io})\,\Delta\theta_i-V_{io}\sin(\delta_{io}-\theta_{io})\,\Delta I_{qi}-I_{qio}\sin(\delta_{io}-\theta_{io})\,\Delta V_i-$$
$$I_{qio}V_{io}\cos(\delta_{io}-\theta_{io})\,\Delta\delta_i+I_{qio}V_{io}\cos(\delta_{io}-\theta_{io})\,\Delta\theta_i-\left[\sum_{k=1}^{n}V_{ko}Y_{ik}\sin(\theta_{io}-\theta_{ko}-\alpha_{ik})\right]\Delta V_i$$
$$-V_{io}\sum_{k=1}^{n}[Y_{ik}\sin(\theta_{io}-\theta_{ko}-\alpha_{ik})]\Delta V_k-\left[V_{io}\sum_{k=1,\neq i}^{n}V_{ko}Y_{ik}\cos(\theta_{io}-\theta_{ko}-\alpha_{ik})\right]\Delta\theta_i$$
$$+V_{io}\textstyle\sum_{k=1,\neq i}^{n}[V_{ko}Y_{ik}\cos(\theta_{io}-\theta_{ko}-\alpha_{ik})]\,\Delta\theta_k+\frac{\partial Q_{li}(V_i)}{\partial V_i}\Delta V_i=0\quad,\qquad(61)$$

and in compact form for all $i=1,\ldots,4$ as

$$0=\underline{C}_2\Delta\underline{x}+\underline{D}_3\Delta\underline{I}_g+\underline{D}_4\Delta\underline{V}_g+\underline{D}_5\Delta\underline{V}_l\,,\qquad(62)$$

The load bus network equations from (9) and (10) are linearized as:

$$0=\tfrac{\partial P_{Li}(V_i)}{\partial V_i}\Delta V_i-[\textstyle\sum_{k=1}^{n}V_{ko}Y_{ik}\cos(\theta_{io}-\theta_{ko}-\alpha_{ik})]\Delta V_i+\left[\sum_{k=1,\neq i}^{n}V_{io}V_{ko}Y_{ik}\sin(\theta_{io}-\theta_{ko}-\alpha_{ik})\right]\Delta\theta_i-$$
$$V_{io}\textstyle\sum_{k=1}^{n}[Y_{ik}\cos(\theta_{io}-\theta_{ko}-\alpha_{ik})]\Delta V_k-V_{io}\sum_{k=1,\neq i}^{n}[V_{ko}Y_{ik}\sin(\theta_{io}-\theta_{ko}-\alpha_{ik})]\,\Delta\theta_k,\qquad(63)$$

$$0=\tfrac{\partial Q_{Li}(V_i)}{\partial V_i}\Delta V_i-[\textstyle\sum_{k=1}^{n}V_{ko}Y_{ik}\sin(\theta_{io}-\theta_{ko}-\alpha_{ik})]\Delta V_i-\left[\sum_{k=1,\neq i}^{n}V_{io}V_{ko}Y_{ik}\cos(\theta_{io}-\theta_{ko}-\alpha_{ik})\right]\Delta\theta_i-$$
$$V_{io}\textstyle\sum_{k=1}^{n}[Y_{ik}\sin(\theta_{io}-\theta_{ko}-\alpha_{ik})]\Delta V_k-V_{io}\sum_{k=1,\neq i}^{n}[V_{ko}Y_{ik}\cos(\theta_{io}-\theta_{ko}-\alpha_{ik})]\,\Delta\theta_k\,,\qquad(64)$$

where $\Delta\underline{V}_{li}=\begin{bmatrix}\Delta\theta_i\\ \Delta V_i\end{bmatrix}$ for $i=5,..,10$,

They can be written in compact form as

$$\underline{0} = \underline{D_6}\Delta\underline{V_g} + \underline{D_7}\Delta\underline{V_l}\ , \tag{65}$$

In summary, the linearized system model can be written in compact form as follows:

$$\Delta\dot{\underline{x}} = \underline{A_1}\Delta\underline{x} + \underline{B_1}\Delta\underline{I_g} + \underline{B_2}\Delta\underline{V_g} + \underline{E_1}\Delta\underline{u}\ , \tag{66}$$
$$\underline{0} = \underline{C_1}\Delta\underline{x} + \underline{D_1}\Delta\underline{I_g} + \underline{D_2}\Delta\underline{V_g}\ , \tag{67}$$
$$\underline{0} = \underline{C_2}\Delta\underline{x} + \underline{D_3}\Delta\underline{I_g} + \underline{D_4}\Delta\underline{V_g} + \underline{D_5}\Delta\underline{V_l}\ , \tag{68}$$
$$\underline{0} = \underline{D_6}\Delta\underline{V_g} + \underline{D_7}\Delta\underline{V_l}\ , \tag{69}$$

To calculate the system matrices, we will need the initial conditions taken as the steady state power flow solution for the states $\delta_{io}, \omega_{io}, E'_{qio}, E'_{dio}, E_{fdio}, I_{dio}, I_{qio}, V_{io}, \theta_{io}, T_{Mio}$, and the Y_{BUS} matrix obtained from the network data.

Referring to Figure 20, the initial condition calculations are computed using the following steps , and machine 1 will be taken as an example.

$$P_{G1} = P_1 - P_{L1}\ and\ Q_{G1} = Q_1 - Q_{L1} \tag{70}$$

$$\bar{I}_{G1} = \frac{P_{G1} - jQ_{G1}}{\bar{V}_1^*} = \frac{7 - j1.3386}{1.03\angle -8.2154} = 6.9193\angle -2.6105$$

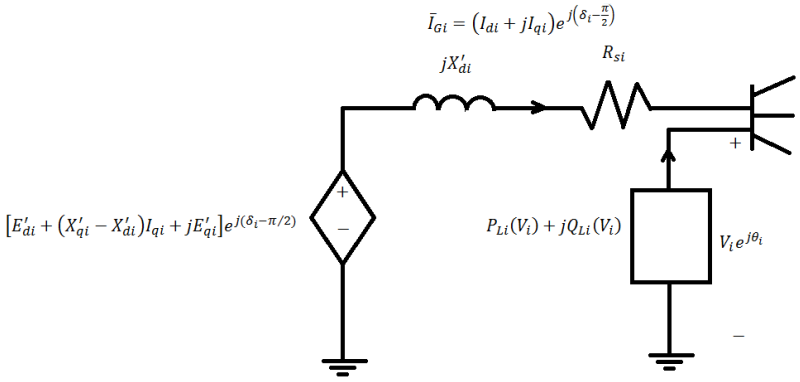

Figure 7: Equivalent Circuit for 2-axis model machine in steady state

In the steady-state condition, all the derivatives (left hand side) of the model (4-8) are equal to zero. Using equation obtained from (7), we obtain

$$E'_{d1} = \left(X_{q1} - X'_{q1}\right) I_{q1} \,. \tag{71}$$

Substituting (69) in the stator algebraic equations (9) and (10) in complex form we get:

$$\begin{aligned} & V_1 e^{j\theta_1} + (R_{s1} + jX'_{d1})\left(I_{d1} + jI_{q1}\right) e^{j\left(\delta_1 - \frac{\pi}{2}\right)} \\ & -\left[\left(X_{q1} - X'_{q1}\right) I_{q1} + \left(X'_{q1} - X'_{d1}\right) I_{q1} + jE'_{q1}\right] e^{j\left(\delta_1 - \frac{\pi}{2}\right)}, \end{aligned} \tag{72}$$

The above equation can be simplified and $\left(I_{d1} + jI_{q1}\right) e^{j\left(\delta_1 - \frac{\pi}{2}\right)}$ is replaced by $\bar{I}_{G1}$, to eventually lead to the following:

$$V_1 e^{j\theta_1} + \left(R_{s1} + jX_{q1}\right) \bar{I}_{G1} = \left[\left(X_{q1} - X'_{d1}\right) I_{q1} + jE'_{q1}\right] e^{j(\delta_1)} \,. \tag{73}$$

The right hand side of the equation is the voltage behind the impedance $\left(R_{s1} + jX_{q1}\right)$ and has an angle of δ_1. Therefore,

$$\begin{aligned} \delta_{1o} &= angle\left(V_1 \angle \theta_1 + \left(R_{s1} + jX_{q1}\right) \bar{I}_{G1}\right) \\ &= angle(1.03 \angle 8.2154 + (0.00028 + j0.19) 6.9192 \angle -2.6105) \\ &= 53.7549\ degrees = 0.9382\ rad \end{aligned} \tag{74}$$

After getting δ_{1o}, we can calculate $I_{d1}$and I_{q1} as follows:

$$\begin{aligned} I_{d1} + jI_{q1} &= \bar{I}_{G1} \angle -\delta_{1o} + \frac{\pi}{2} \\ &= 6.9192 \angle 33.6349^o \quad pu \\ I_{d1o} &= 6.9192 \cos(33.6349) = 5.7608 \quad pu \\ I_{q1o} &= 6.9192 \sin(33.6349) = 3.8325 \quad pu \end{aligned}$$

We know that

$$\left(V_{d1} + jV_{q1}\right)\angle(\delta_{1o} - 90) = V_1\angle\theta_1\ , \tag{75}$$

Therefore

$$\begin{aligned} V_{d1} + jV_{q1} &= V_1\angle\theta_1 - \delta_{1o} + 90 \\ &= 1.03\angle 44.4605^o \\ V_{d1o} &= 1.03cos(44.4605) = 0.7324 \quad pu \\ V_{q1o} &= 1.03sin(44.4605) = 0.7242 \quad pu \end{aligned}$$

From equation (69), we have

$$\begin{aligned} E'_{d1o} &= \left(X_{q1} - X'_{q1}\right)I_{q1} \\ &= (0.19 - 0.061)3.8325 = 0.4972 \quad pu \end{aligned}$$

Using the stator equations (9), (10) and substituting E'_{d1} from equation (73) we get

$$\begin{aligned} E'_{q1o} &= V_{q1} + R_{s1}I_{q1} + X'_{d1}I_{d1} \\ &= 0.72143 + 0.00028 * 3.8325 + 0.033 * 5.7608 \\ &= 0.9149 \quad pu \end{aligned}$$

For the steady state condition obtained from equation (8), we get

$$\begin{aligned} E_{fd1o} &= E'_{q1} + (X_{d1} - X'_{d1})I_{d1} \\ &= 0.9149 + (0.2 - 0.033)5.7608 \\ &= 1.8746 \quad pu \end{aligned}$$

The initial conditions for the rest of the machines will be carried in a similar manner, and all the results are shown in the Table 2.

Table 2: Initial conditions of the machines states

Variable / Machine	Machine 1	Machine 2	Machine 3	Machine 4
$\delta_{io}(rad)$	0.9344	0.7619	0.7985	0.5948
$I_{dio}(pu)$	5.7462	6.0259	5.9993	6.1208
$I_{qio}(pu)$	3.8546	3.7693	3.8832	3.7115
$V_{dio}(pu)$	0.7324	0.7162	0.7378	0.7052
$V_{qio}(pu)$	0.7242	0.7122	0.7187	0.7231
$E'_{dio}(pu)$	0.4972	0.4862	0.5009	0.4788
$E'_{qio}(pu)$	0.9149	0.9121	0.9178	0.9261
$E_{fdio}(pu)$	1.8746	1.9184	1.9196	1.9483

Since is $\Delta\underline{I_g}$ an algebraic variable, it is not of interest and can be eliminated. Reordering (69) to

$$\Delta\underline{I_g} = -\underline{D_1}^{-1}\underline{C_1}\Delta\underline{x} - \underline{D_1}^{-1}\underline{D_2}\Delta\underline{V_g} \ , \tag{76}$$

And substitute it into (70) to get:

$$\underline{0} = \underline{K_2}\Delta\underline{x} + \underline{K_4}\Delta\underline{V_g} + \underline{D_5}\Delta\underline{V_l}, \tag{77}$$

where

$$\underline{K_1} = \underline{D_4} - \underline{D_3}\underline{D_1}^{-1}\underline{D_2}, \tag{78}$$
$$\underline{K_2} = \underline{C_4} - \underline{D_3}\underline{D_1}^{-1}\underline{C_1}, \tag{79}$$

We write the system now as in Equations (68)-(71) can be written in matrix form as following:

$$\begin{bmatrix}\Delta\underline{\dot{x}}\\ 0\end{bmatrix} = \begin{bmatrix}\underline{A'} & \underline{B'}\\ \underline{C'} & \underline{D'}\end{bmatrix}\begin{bmatrix}\Delta\underline{x}\\ \Delta\underline{V_N}\end{bmatrix} + \begin{bmatrix}\underline{E_1}\\ \underline{0}\end{bmatrix}\Delta\underline{u}, \tag{80}$$

where $\Delta\underline{V_N} = \begin{bmatrix}\Delta\underline{V_g}\\ \Delta\underline{V_l}\end{bmatrix}$,

Usually in the calculation in power systems, one rotor angle of a generator is taken as a reference for the other rotor angles. This makes representing the reference state redundant, and a common procedure is to eliminate that state from the system. If the state is not eliminated, this results in a zero eigenvalue for the state matrix. The latter case is considered in our simulations, and we simply neglect the additional zero eigenvalue (we actually get two because the damping for the generators is taken to be zero, and this will be seen later). Now we can get the reduced system as

$$\Delta\underline{\dot{x}} = \underline{A}_{sys}\Delta\underline{x} + \underline{E}\Delta\underline{u}, \tag{81}$$

where $\underline{A}_{sys} = \underline{A}' - \underline{B}'\underline{D}'^{-1}\underline{C}'$. (82)

The eigenvalues of the linearized system $\underline{A}_{sys}$ are shown in Table 3. There are two zero eigenvalues, which is due to the fact that none of the rotor angles of the machines was taken as the reference, and the damping of the system is zero. We can see that the system is originally stable since all the eigenvalues of the system at the equilibrium point have negative real parts.

Table 3: Eigenvalue of linearized system and Participation factor results

Eigenvalues			Frequency (Hz)	Dominant States
No.	Real	Imaginary		
1	-4.4284	∓17.3658i	2.7639	E'_{q4},E_{fd4},E'_{q3},E_{fd3}
2	-5.0993	∓11.6539i	1.8548	E'_{q1},E_{fd1},E'_{q2},E_{fd2}
3	-5.3479	∓6.9711i	1.1095	E'_{q1},E_{fd1},E'_{q2},E_{fd2}
4	-5.2847	∓7.2880i	1.1599	E'_{q4},E_{fd4},E'_{q3},E_{fd3}
5	-0.7626	∓7.5073i	1.1948	δ_1, ω_1, δ_2, ω_2
6	-0.7744	∓6.8311i	1.0872	δ_3, ω_3, δ_4,ω_4
7	-0.0159	∓4.6172i	0.7348	δ_3, ω_3, δ_1, ω_1
8	-4.3092	0	0	E'_{d1}
9	-4.5295	∓0.0853i	0.0136	E'_{d2},E'_{d3}
10	-4.6810	0	0	E'_{d4}
11	0	0	0	-
12	0	0	0	-

In order to identify the nature of the mode of oscillation, whether local or interarea, we use the same criteria as used before which is depending on the characteristics of the right eigenvector for each eigenvalue. The electromechanical modes are the dominant modes in the system and the most contributing in the modes of oscillation and coherent grouping. Therefore, we focus our analysis only on those modes. We are able to identify the electromechanical modes through the participation factor from the following equation:

$$p_{ki} = \frac{w_{ki} v_{ki}}{\underline{w}_i^t \underline{v}_i} \qquad for\ i,k = 1, \dots, 20, \tag{83}$$

where $\underline{v}_i$, $\underline{w}_i^t$ are the right and left eigenvectors, for mode i, respectively. The left eigenvectors are obtained from

$$\underline{W}^t = \underline{V}^{-1} = \begin{bmatrix} \underline{w}_1^t \\ \vdots \\ \underline{w}_n^t \end{bmatrix}, \tag{84}$$

After the calculation of the participation factor, the dominant states contributing in each be found. The final results of the participation factors calculations are shown in Table 2. Focusing on the modes which have dominant electromechanical modes, we end up with modes {5, 6, and 7}. The plots of the corresponding mode shapes in the phasor plane are shown in Figures (8)-(10).

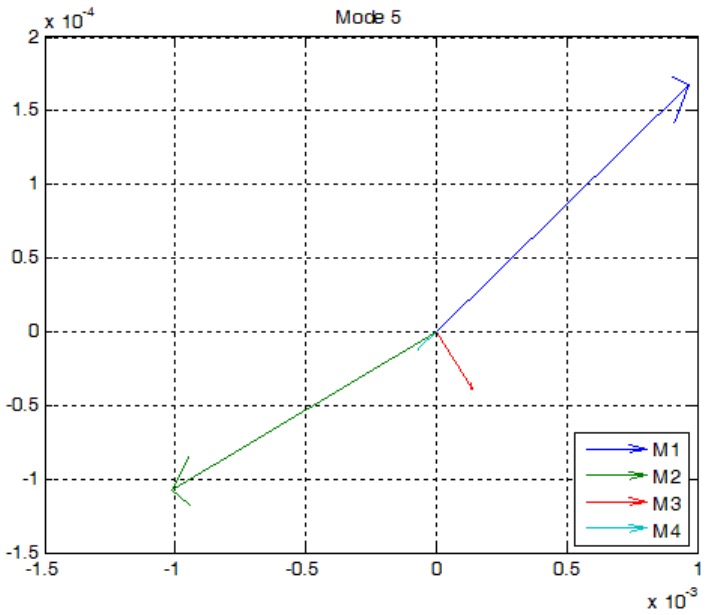

Figure 8: Mode 5 of linearized system

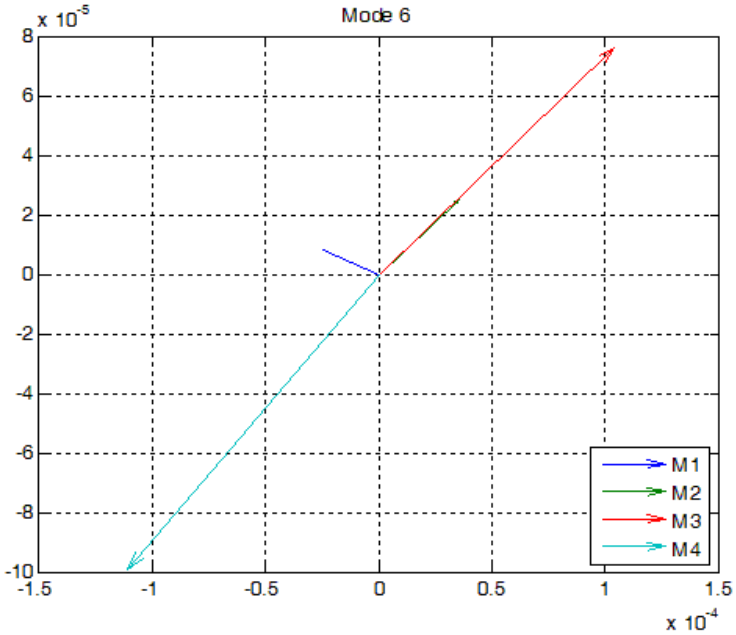

Figure 9: Mode 6 of linearized system

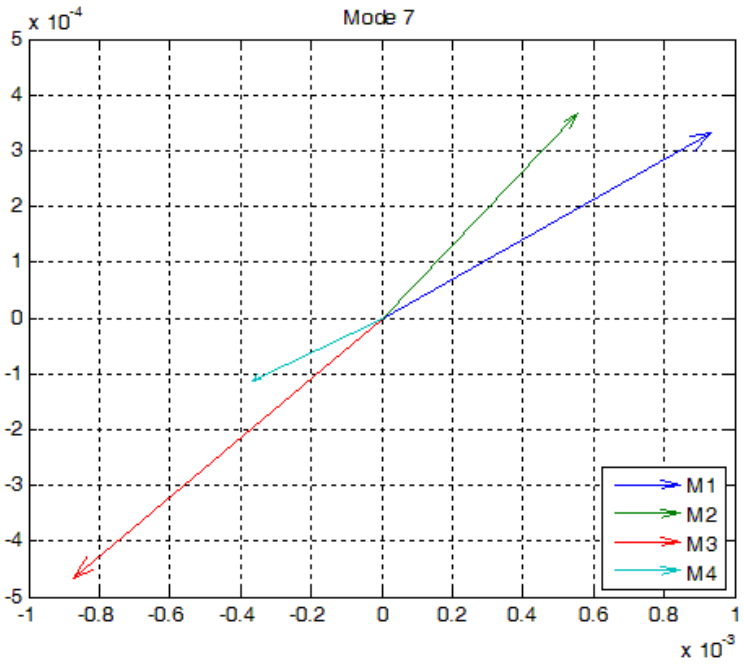

Figure 10: Mode 7 of linearized system

We can observe that mode 5 with frequency 1.1948 Hz is a local mode in area 1, which is dominant in generators 1 and 2, and the fact that expresses different directions in the phasor plot for the two machines. We can also see that mode 6 with frequency 1.0872 Hz is local mode but in area 2 with its dominant states are generators 3 and 4 electromechanical states, and that it shows different direction for the mode shape in the phasor plot. On the other hand, we can identify mode 7 with frequency 0.7348 Hz to be an interarea mode by noticing that it is dominant in both area and the eigenvectors for each area of generators is pointing in a similar direction, opposite to the direction of the other area. It can be considered in local modes as the machines are swinging against each other in the same area. However, for an interarea mode, it can be considered as the machines of each area are swinging together against the machines from the other area.

In comparison of the two methods of analysis, the KMA gives us an extension of the small-signal stability analysis in terms of decomposing the system into modes with single frequency of oscillation with and association eigenvector (Koopman mode) to describe the behavior of each

mode with respect to each system state (observable). The KMA can provide more reliable results when the system is not operating in the neighborhood of the equilibrium operating point and.

The small-signal stability analysis does not depend on the disturbance, it relies on the system model and intrinsic characteristics. On the other hand, KMA can capture linear and nonlinear modes in the system but, however, these modes need to be excited by the disturbance in order to be captured.

4.2 IEEE Thirty Nine Bus System

4.2.1 Koopman Mode Analysis for 39-Bus System

We apply KMA to analyze the swing-dynamics of the system. Figure 11 shows the 39-bus system which contains 10 generators, transformers and transmission lines, represented by single line diagram. The details for the system data is provided in [29]. The model used for the generators is the classical model described in chapter 2.

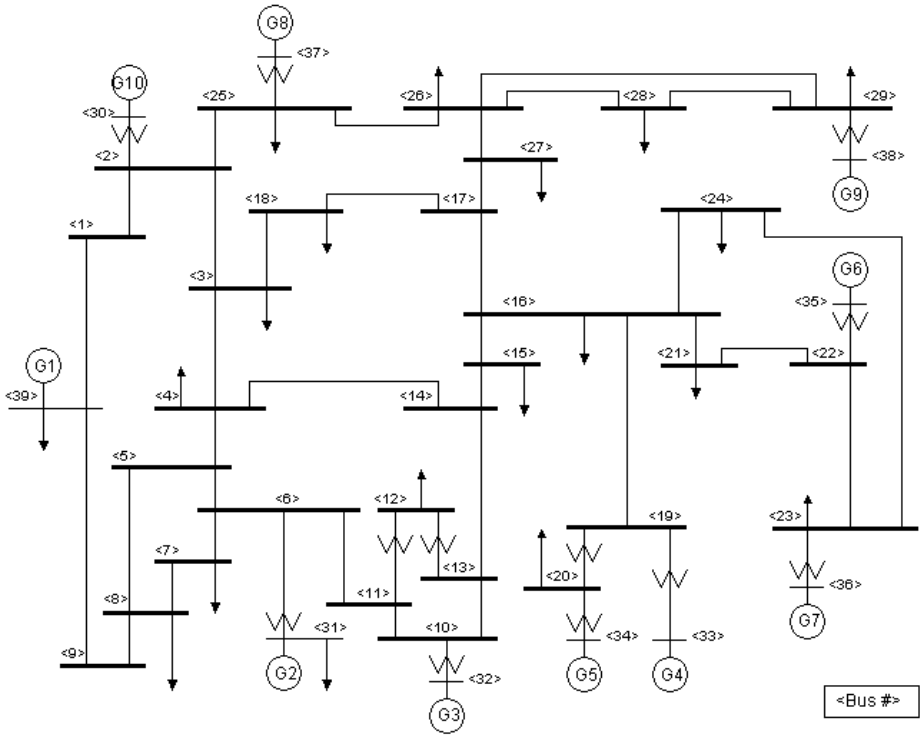

Figure 11: 39 bus system

All simulations have been performer using MATLAB, with numerical integration for the system differential equation with a step of $T = 0.02$ seconds (sampling frequency 50 Hz). After solving the system for equilibrium point using power flow solution, a local disturbance at generator 8 is applied by using the following initial conditions:

$$(\delta', \omega') = \begin{Bmatrix} \delta'_{8o} = \delta_{8o} + 1.0 \\ \omega'_{8o} = \omega_{8o} + 3.0 \end{Bmatrix}.$$

These initial conditions are used to emulate the disturbance caused by a three-phase fault at bus 37, corresponding to internal bus of generator eight. The simulation results of the swing equation are shown in Figure 12. From the figure, we can see that after clearing the disturbance by few seconds, the system is showing bounded oscillations.

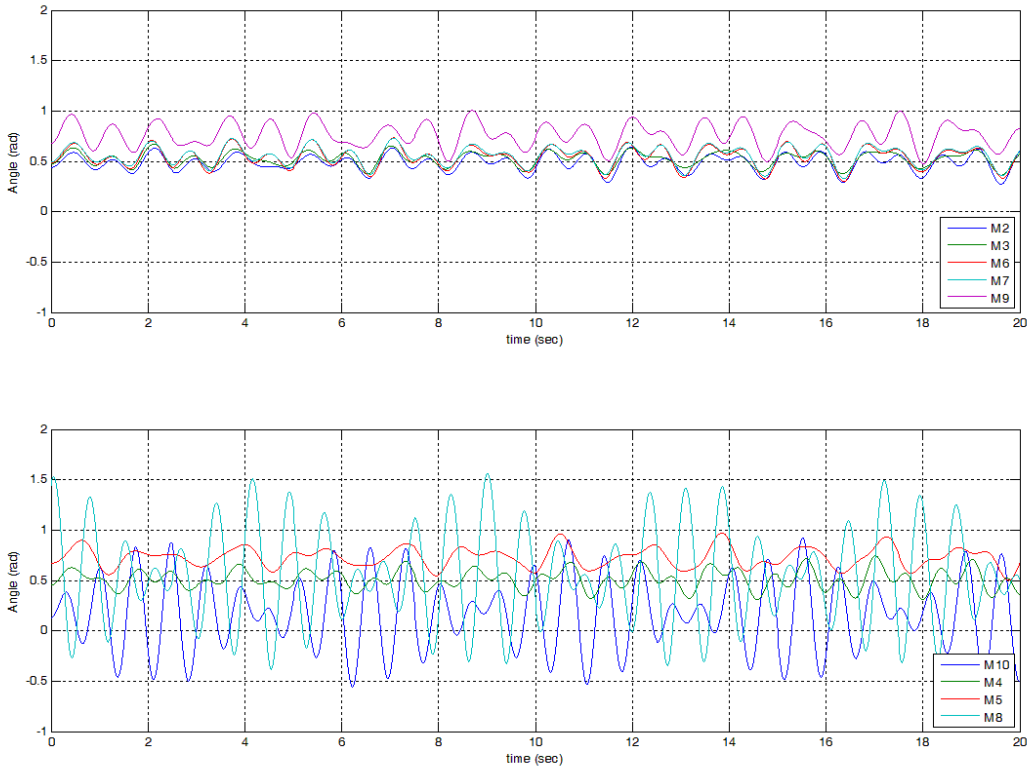

Figure 12: Stable oscillations in 39 bus system

By applying Discrete Fourier Transform (DFT) to the swing dynamics, we obtain the depicted graph in Figure 13. Some clean peaks are observed in the frequency spectrum of each machine. These peaks represent the dominant frequencies with highest energy in the system, with respect to each machine. From Figure 13, we can see that the system has three main frequencies dominating the electromechanical swing dynamics. These frequencies are: 1) 0.586 Hz obtained from all machines beside 8, 2) 1.27 Hz from machines 2, 3, 6-10, and 3) 1.47 Hz from machines 4,8,10. These results will be used to check the output of the KMA.

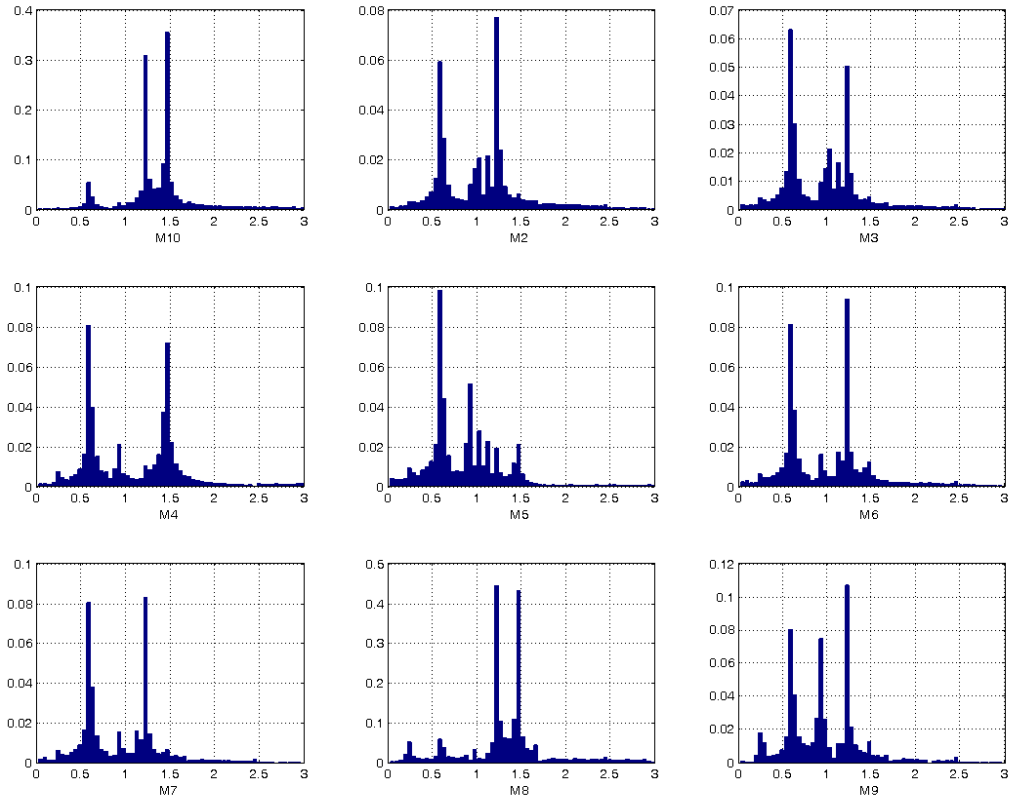

Figure 13: Discrete Fourier Transform

Now, we apply the KMA using the Arnoldi method to swing dynamics of the rotor angle and speed for all machines to compute the Ritz values $\tilde{\lambda}_j = r_j e^{i\theta_j}$, and the associated vectors $\tilde{v}_j$. The modes that are taken into consideration are the ones with the highest norm and growth rate. The results in table 4 show each mode with its growth rate, frequency defined as $\theta_j/2\pi T$ and the norm defined as $||\tilde{v}_j||$. These modes represent sustained swing components in the simulation output studied and have dominant magnitudes in the output. We can double check the results by identifying that the results also included the frequencies 0.586, 1.26, 1.45 Hz which were similarly captured by DFT.

Table 4: Koopman Mode analysis for 39-bus system

Mode	Lambda	Frequency	Growth rate	Norm
1	0.9959 - 0.0345i	0.2757	0.9965	0.130548
2	0.9951 - 0.0468i	0.3736	0.9961	0.094652
3	0.9985 - 0.0737i	0.5860	1.001	0.173478
4	0.9928 - 0.1149i	0.9165	0.9994	0.355926
5	0.9918 - 0.1261i	1.006	0.9997	0.236211
6	0.9849 - 0.1820i	1.4537	1.001	1.609743
7	0.9904 - 0.1411i	1.125	1.000	0.164667
8	0.9883 - 0.1550i	1.237	1.000	2.687459
9	0.9867 - 0.1578i	1.261	0.9992	1.090059

Now we proceed to coherency identification for the generators. Figures (14)-(16) shows the representation of the KMs components in the phasor plane. We can identify coherent grouping with respect to the modes. We can notice that for mode 3 with frequency 0.586 Hz, all machines excluding 8 and 10 are expressing similar characteristics in terms of magnitude and phase. Similar to this criterion, we can conclude that machines 2-7, 9 are coherent with respect to mode 8, and that mode 6 is not experiencing any coherent grouping since machines 8 and 10 are showing completely different directions in the phasor plane. This can be checked also by comparing the results with the swings for the rotor angle (speed) grouped together for clarification in Figure 11. In a similar manner using this criterion, a clustering algorithm can be used to automatically identify and group coherent machines.

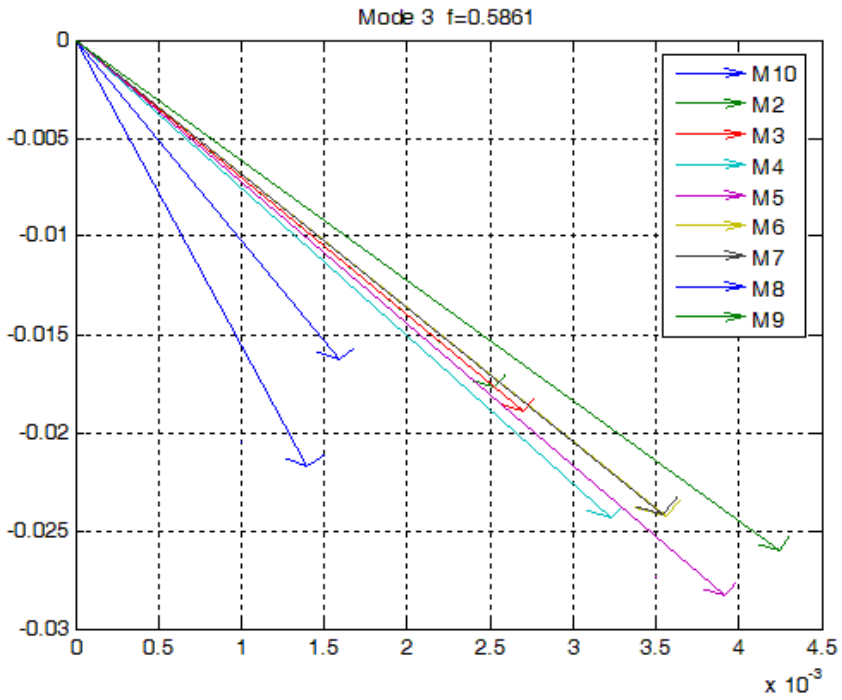

Figure 14: Mode 3 phasor plot

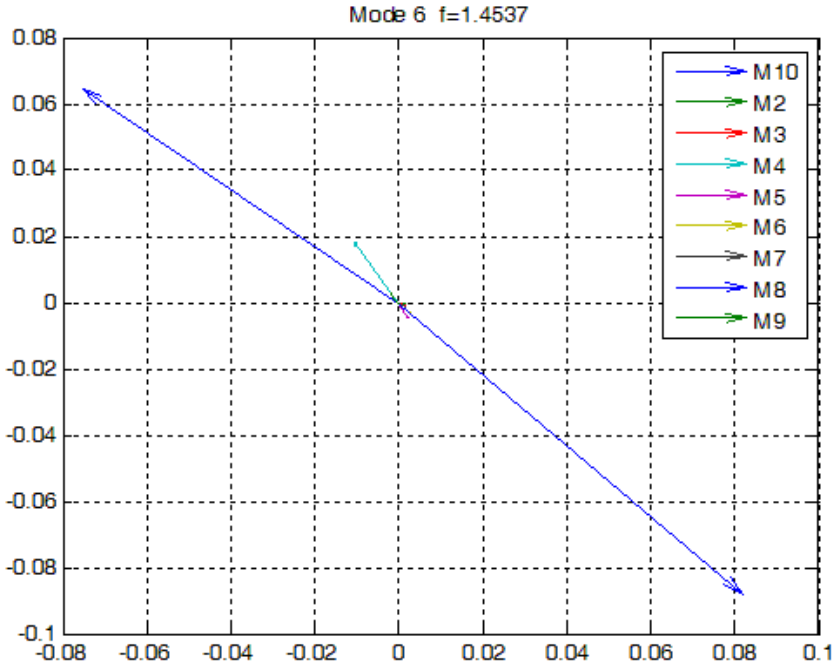

Figure 15: Mode 6 phasor plot

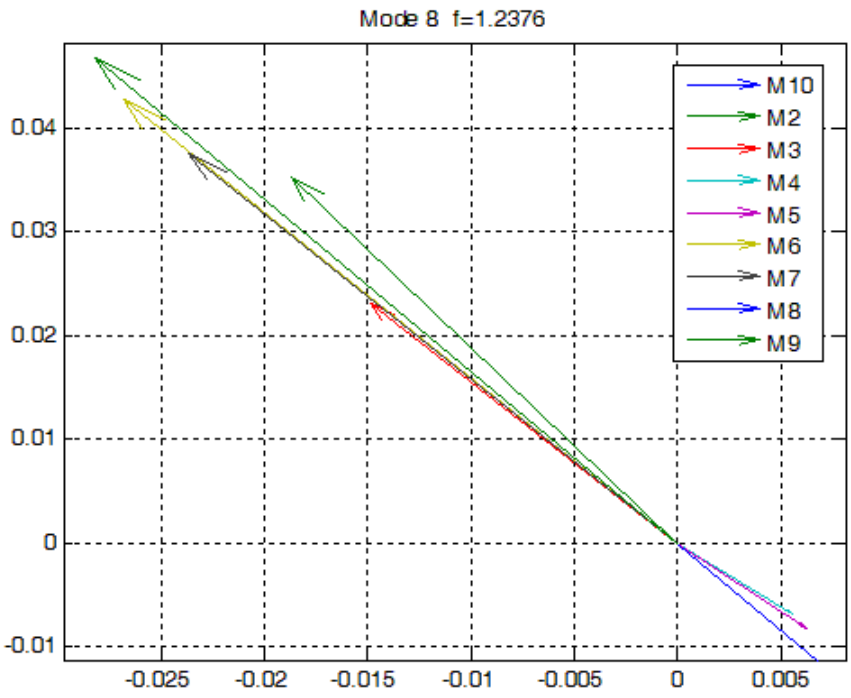

Figure 16: Mode 8 phasor plot

4.2.2 Different Fault Locations

We will use this method to analyze the system for different fault locations. Table 5 shows the results for each case.

Table 5: Grouping results from different fault locations

Modes/	0.57 Hz		0.85 HZ		0.97 HZ		1.07 Hz		1.16 Hz		1.35 Hz	
Fault Loc	G 1	G 2	G 1	G 2	G1	G 2	G 1	G 2	G 1	G 2	G1	G 2
2	all	-	-	-	2,3	5,9	-	-	-	-	-	-
3	all	-	-	-	2,3	5,9	-	-	-	-	-	-
4	all	-	-	-	-	-	-	-	-	-	2,3,5,6,7,9	4
5	all	-	-	-	2,3,6,7	5,9	-	-	-	-	-	-
6	all	-	-	-	-	-	2,3,5	6,7	-	-	-	-
7	all	-	-	-	-	-	2,3,5	6,7	-	-	-	-
9	all	-	2-6,7	9	-	-	-	-	-	-	-	-
10	all	-	-	-	-	-	-	-	2,3,6,7,9	8,10	-	-

We can see that through the KMA, we are able to identify certain grouping in the system. All the machines tend to group together with respect to 0.57 Hz frequency mode. Even by changing the fault location and the strength of the fault, the machines maintained the grouping with respect to this mode. This can be understood as the KMA was able to identify some inherent natural frequencies in the system.

Moreover, machines {2,3} and {6,7} tend to always group together regardless of the fault location. It can be explained due to the electrical proximity of the machines to each other. Also, machines 2,3,6 and 7 do form a group, with respect to a certain mode that change with different fault location, as long as the fault is not applied on any of them. However, the same does not apply for machines 4,5 - even their electrical closeness does not lead to the machines swinging together after any disturbance. This can be due to the presence of the load on bus 20, which leads to decouple these two generators.

4.2.3 Precursor to Instability

In this case we study the system under unstable condition. The system is disturbed with a fault at machine bus 8. For 7 seconds after the fault was cleared, the system is not showing any signs of instability. However, after 8 seconds the generators' rotor angles start growing until they lose synchronism with the infinite bus. The simulation results for the generators' rotor angles are shown in Figure 17. The fault was simulated by applying a stronger disturbance at generator 8 compared with the fault applied in the previous case. Different initial conditions are used to simulate this disturbance, which are

$$(\delta', \omega') = \begin{Bmatrix} \delta'_{8o} = \delta_{8o} + 1.93 \\ \omega'_{8o} = \omega_{8o} + 3.0 \end{Bmatrix}$$

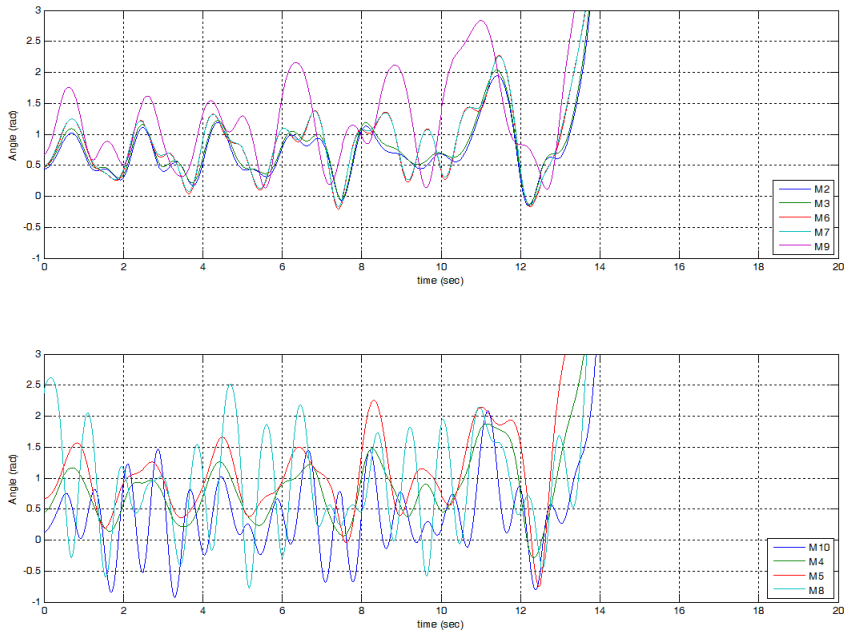

Figure 17: Unstable disturbance for 39-bus system

We will use the action-angle representation developed in chapter 3 to find a precursor to system instability. The action-angle representation is a reduced order model of the system in terms of the dominant modes. Therefore, with the KMA and the reduced system model we are able to predict

the system behavior for the next few seconds and determine if the system will maintain stability. This can be seen as one (or more) mode start to grow largely until it diverges and, consequently, destabilizes the system.

We start the analysis by the computation of Koopman modes using Arnoldi method. The dominant modes in the short-term swings are listed in Table 6 with their growth rates, frequencies and norms.

Table 6: Koopman Mode analysis for an unstable disturbance

Mode	Lambda	Frequency	Growth rate	norm
1	0.9985 - 0.0737i	0.5861	1.001	0.1735
2	0.9928 - 0.1149i	0.9165	0.9994	0.3559
3	0.9918 - 0.1261i	1.006	0.9998	0.2362
4	0.9849 - 0.1820i	1.454	1.006	1.610
5	0.9904 - 0.1411i	1.126	1.000	0.1647
6	0.9867 - 0.1578i	1.262	0.9993	1.090

We will now calculate the action-angle for these dominant modes. The results of the growth rate for the modes are shown in Figure 18. We can notice that mode 1 starts with very large amplitude and keeps growing until it becomes unstable and ultimately destabilizes the rest of the system. This can be considered as predicting the behavior of these modes after a few seconds of the disturbance, and evaluating the system's stability. This phenomena has been also explained by [17] in terms of transfer of energy. The authors show that the system lose stability due to the transfer of energy from high frequency modes to the low frequency modes, which leads to the amplitude of the latter continuously growing until the system loses stability.

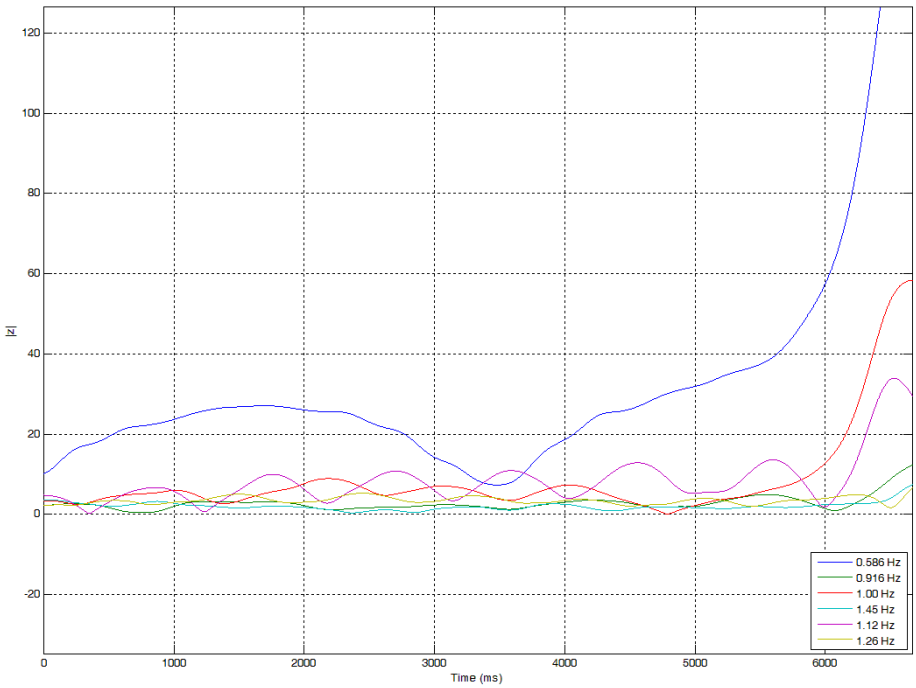

Figure 18: Action-angle variables progress with time

We now verify that the dominant modes of oscillation do not depend on the machine model. Hence, the classical model would be sufficient to find the coherent oscillations and machines. The following simulation has used the two-axis model developed in chapter 2 for the 39-bus 10 machine system. The swings dynamics of the generators are studied by applying a fault with duration of $160\ ms$ at bus 37. The rotor angles oscillations are shown in Figure 19.

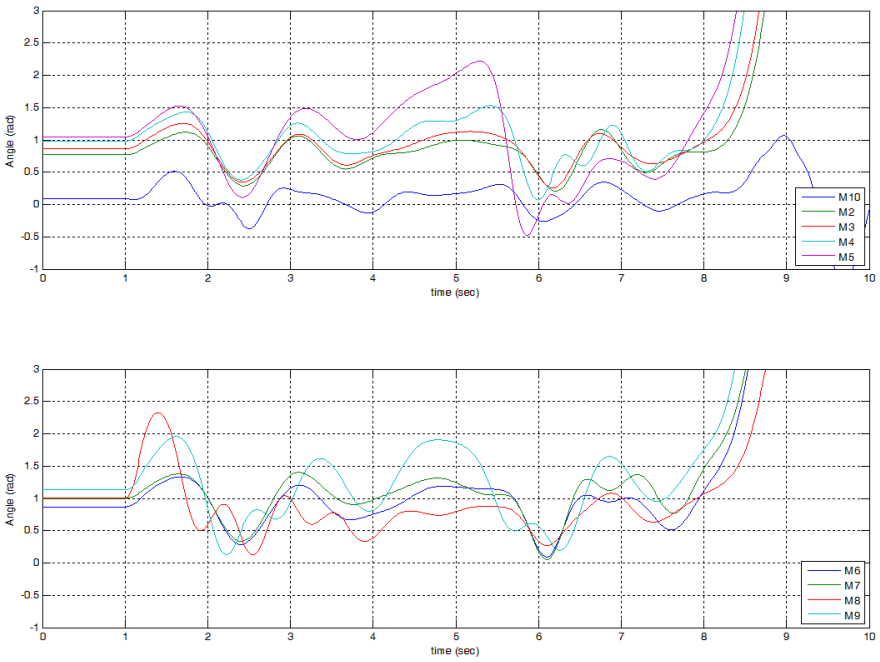

Figure 19: Rotor angles dynamics for 39-bus system with 2-axis model

The DFT analysis for these swings will help us identify the frequencies of oscillation. The results of the DFT are shown in Figure 20.

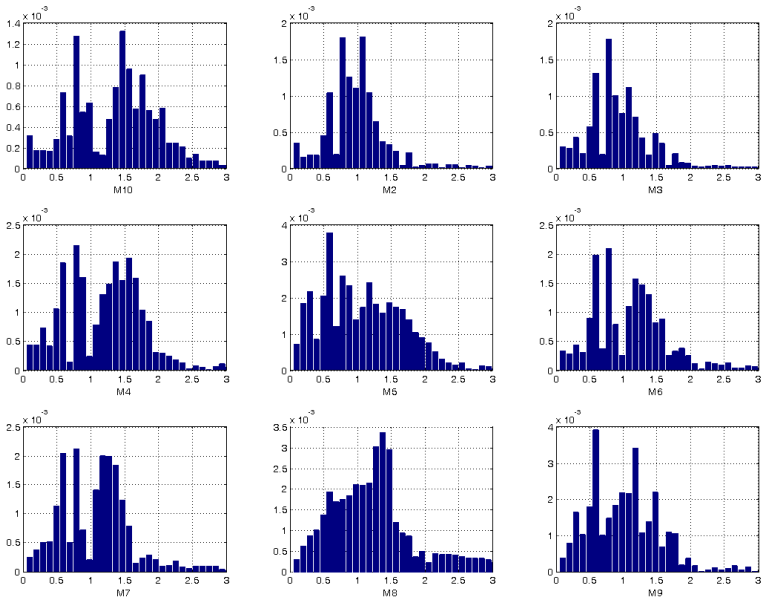

Figure 20: DFT for rotor angle dynamics for 39-bus system with 2-axis model

By applying the KMA to the states of the system represented by $\{V_{ti}, \delta_i, E_{fdi}, I_{ti}, \omega_i\}$ for $i = 1, \ldots, 10$, we will obtain the KMs with their associated frequencies of oscillations and growth rates. Table 7 shows the results for eigenvalues of each mode and their characteristics.

Table 7: KMA for 39-bus system with 2-axis model

Mode	Eigenvalues	Frequency	Growth Rate	Norm
1	0.9989 - 0.1436i	1.136	1.009	1.274
2	0.9885 - 0.1236i	0.9899	0.9961	11.47
3	0.9967 - 0.0684i	0.5449	0.9990	35.86
4	0.9981 - 0.0323i	0.2575	0.9986	37.52
5	1.0018 - 0.0064i	0.05078	1.002	37.45
6	0.9901 - 0.1013i	0.8116	0.9952	23.74
7	1.0041 - 0.1017i	0.8036	1.009	1.152

The frequencies that were found using DFT have small differences with the ones obtained using KMA. This can be explained as the DFT is applied only on one state which in this case is the rotor angle for the generators. However, the KMA is applies on all system states. These states have some interactions between each other and this will have an impact on the system modes of oscillation. The variations in the frequencies of oscillation are small which shows that the dominant modes in power systems are the electromechanical modes, namely the machines rotor angles and speeds. It is clear that the modes (frequencies) captured by the KMA for the generators represented by the two-axis model are very similar to the ones found for the same system with the classical model. This analysis can help us conclude that to study coherent swings and machines in power systems, a classical model for the generators will be sufficient. The detailed model will definitely be more realistic because they include the generators controllers. However, these controllers will affect mainly the damping of the oscillations and it will have an insignificant effect on the oscillations frequencies.

Chapter 5 – Conclusions and Future Work

We carried out modal analysis for swing dynamics of a power system using KMA. This method was applied on two systems, namely the four-machine two-area system and the 39-bus system. Since the KMA is based on observables which can be obtained from simulations or real-time measurements, it does not rely on any mathematical models of the system. We have shown that the KMA identifies single-frequency oscillatory modes from transient data samples under various operating conditions of a system, including the case where the operating point is off-attractor following the application of a large disturbance. Small-signal stability analysis has been applied to two test systems and its results compared to those obtained from KMA. Unlike conventional methods such as small-signal stability analysis, the POD, or the weak coupling method, the KMA captures all the nonlinearities in the system since no linearization of the power system model is performed. The KMA also extracts inherent dynamics in the system response. We show that the KMA offers an effective way for mode identification in transient dynamics.

The main purpose of this modal analysis is identification of coherent machines. We have shown that the coherency identification process using KMA is disturbance dependent. Due to the nonlinearities in the system, different modes are excited for different fault locations. In contrast, the conventional small-signal stability is fault-independent since it relies on the linearization of the system model around stable equilibria. Since KMs are defined for nonlinear dynamical systems, different operating conditions yield different KMs. Nevertheless, system operating points evolving within the same basin of attraction have the same KMs.

Here, the KM computation has been carried out using an Arnoldi-based method. Unlike a Fourier-based method, which may be utilized instead for operating points on-attractor as discussed in [16], an Arnoldi-based method provides more accurate calculation of the KMs when the operating point is off-attractor.

The action-angle representation provides a model reduction tool for the dominant system oscillatory modes. It describes the interaction between the nonlinear KMs that are found by monitoring the evolution of the system states. After the calculation of the KMs, an off-line analysis can be carried out using the action-angle operator and the system mathematical model to detect system instability. While this representation has been used for the case of CSI[28], it can be developed for any other system instability. In [30]the authors apply the Koopman mode analysis to detect an instability based on data of power flows sampled from two major accidents, the 2011 Arizona-Southern California grid outage and the 2006 system disturbance of the European power grid. In their analysis they were able to successfully detect unstable power flow patterns that describe the complex dynamics that occur during and after disturbances.

As future work, we intend to seek more efficient way for calculating a selected subset of eigenvalues of the companion matrix. In the current analysis, all the eigenvalues are calculated while only few of them are of interest to determine the growth rate and the norms of the KMs values. By using the DFT, the frequencies of the modes can be used as an initial guess to find the eigenvalues associated with these frequencies only, which will save computing time and make the approach more efficient.

Another future research task is to carry out a KMA on power systems with embedded microgrids and FACTS devices. The fact that this technique relies only on data measurements makes it very attractive for stability analysis of power systems that include, for example, Photovoltaic (PV) cells and wind turbines with their converters. Using only data samples obtained from measurements of the system, it is possible to perform modal analysis for these systems without resorting to complex mathematical model.

References

[1] E. H. Abed and P. P. Varaiya, "Nonlinear oscillations in power systems," *International Journal of Electrical Power & Energy Systems,* vol. 6, pp. 37-43, 1984.

[2] J. Winkelman, J. Chow, B. Bowler, B. Avramovic, and P. Kokotovic, "An analysis of interarea dynamics of multi-machine systems," *Power Apparatus and Systems, IEEE Transactions on,* pp. 754-763, 1981.

[3] P. P. Varaiya, F. F. Wu, and M. G. Lauby, "Chaos in a Simple Power System," *IEEE Transactions on Power Systems,* vol. 8, p. 1407, 1993.

[4] Q. Chen and L. Mili, "Composite power system vulnerability evaluation to cascading failures using importance sampling and antithetic variates," 2013.

[5] M. Klein, G. Rogers, and P. Kundur, "A fundamental study of inter-area oscillations in power systems," *IEEE Transactions on Power Systems,* vol. 6, pp. 914-921, 1991.

[6] P. W. Sauer and M. Pai, *Power system dynamics and stability* vol. 6: Prentice Hall Upper Saddle River, NJ, 1998.

[7] P. Kundur, J. Paserba, V. Ajjarapu, G. Andersson, A. Bose, C. Canizares, *et al.*, "Definition and classification of power system stability IEEE/CIGRE joint task force on stability terms and definitions," *Power Systems, IEEE Transactions on,* vol. 19, pp. 1387-1401, 2004.

[8] P. M. Anderson and A. A. Fouad, *Power system control and stability*: John Wiley & Sons, 2008.

[9] I. P. S. E. Committee, *Voltage stability of power systems: concepts, analytical tools, and industry experience*: IEEE, 1990.

[10] P. Kundur, N. J. Balu, and M. G. Lauby, *Power system stability and control* vol. 7: McGraw-hill New York, 1994.

[11] R. Podmore, "Identification of coherent generators for dynamic equivalents," *Power Apparatus and Systems, IEEE Transactions on,* pp. 1344-1354, 1978.

[12] J. H. Chow, *Time-scale modeling of dynamic networks with applications to power systems* vol. 46: Springer-Verlag, 1982.

[13] J. Chow, J. Winkelman, M. Pai, and P. Sauer, "Singular perturbation analysis of large-scale power systems," *International Journal of Electrical Power & Energy Systems,* vol. 12, pp. 117-126, 1990.

[14] F. Ma and V. Vittal, "A hybrid dynamic equivalent using ANN-based boundary matching technique," *Power Systems, IEEE Transactions on,* vol. 27, pp. 1494-1502, 2012.

[15] T. B. Nguyen and M. Pai, "Dynamic security-constrained rescheduling of power systems using trajectory sensitivities," *IEEE Transactions on Power Systems,* vol. 18, pp. 848-854, 2003.

[16] D. Chaniotis and M. Pai, "Model reduction in power systems using Krylov subspace methods," *IEEE Transactions on Power Systems,* vol. 20, pp. 888-894, 2005.

[17] S. Liu, "Dynamic-data driven real-time identification for electric power systems," Citeseer, 2009.

[18] G. Verghese, I. Perez-Arriaga, and F. Schweppe, "Selective modal analysis with applications to electric power systems, Part II: The dynamic stability problem," *Power Apparatus and Systems, IEEE Transactions on,* pp. 3126-3134, 1982.

[19] R. Nath, S. S. Lamba, and K. Rao, "Coherency based system decomposition into study and external areas using weak coupling," *Power Apparatus and Systems, IEEE Transactions on,* pp. 1443-1449, 1985.

[20] A. R. Messina and V. Vittal, "Nonlinear, non-stationary analysis of interarea oscillations via Hilbert spectral analysis," *Power Systems, IEEE Transactions on,* vol. 21, pp. 1234-1241, 2006.

[21] P. A. Parrilo, S. Lall, F. Paganini, G. C. Verghese, B. C. Lesieutre, and J. E. Marsden, "Model reduction for analysis of cascading failures in power systems," 1999.

[22] A. Messina and V. Vittal, "Extraction of dynamic patterns from wide-area measurements using empirical orthogonal functions," *Power Systems, IEEE Transactions on,* vol. 22, pp. 682-692, 2007.

[23] I. Mezić, "Spectral properties of dynamical systems, model reduction and decompositions," *Nonlinear Dynamics,* vol. 41, pp. 309-325, 2005.

[24] C. W. Rowley, I. MEZIĆ, S. Bagheri, P. Schlatter, and D. S. Henningson, "Spectral analysis of nonlinear flows," *Journal of Fluid Mechanics,* vol. 641, pp. 115-127, 2009.

[25] Y. Susuki and I. Mezic, "Nonlinear Koopman modes and coherency identification of coupled swing dynamics," *IEEE Transactions on Power Systems,* vol. 26, pp. 1894-1904, 2011.

[26] Y. Susuki and I. Mezic, "Nonlinear Koopman modes and a precursor to power system swing instabilities," *Power Systems, IEEE Transactions on,* vol. 27, pp. 1182-1191, 2012.

[27] A. Ruhe, "Rational Krylov sequence methods for eigenvalue computation," *Linear Algebra and its Applications,* vol. 58, pp. 391-405, 1984.

[28] Y. Susuki, I. Mezić, and T. Hikihara, "Coherent swing instability of power grids," *Journal of nonlinear science,* vol. 21, pp. 403-439, 2011.

[29] M. Pai, *Energy function analysis for power system stability*: Springer, 1989.

[30] Y. Susuki and I. Mezic, "Nonlinear Koopman Modes and Power System Stability Assessment Without Models," 2013.